Gary W. Slater[1]
Christian Holm[2,3]
Mykyta V. Chubynsky[1]
Hendrick W. de Haan[1]
Antoine Dubé[1]
Kai Grass[2]
Owen A. Hickey[1]
Christine Kingsbury[1]
David Sean[1]
Tyler N. Shendruk[1]
Lixin Zhan[1]

[1]Department of Physics,
 University of Ottawa, Ottawa,
 Ontario, Canada
[2]Frankfurt Institute for Advanced
 Studies, JW Goethe Universität,
 Frankfurt, Germany
[3]Max Planck Institute for Polymer
 Research, Mainz, Germany

Review

Modeling the separation of macromolecules: A review of current computer simulation methods

Theory and numerical simulations play a major role in the development of improved and novel separation methods. In some cases, computer simulations predict counterintuitive effects that must be taken into account in order to properly optimize a device. In other cases, simulations allow the scientist to focus on a subset of important system parameters. Occasionally, simulations even generate entirely new separation ideas! In this article, we review the main simulation methods that are currently being used to model separation techniques of interest to the readers of *Electrophoresis*. In the first part of the article, we provide a brief description of the numerical models themselves, starting with molecular methods and then moving towards more efficient coarse-grained approaches. In the second part, we briefly examine nine separation problems and some of the methods used to model them. We conclude with a short discussion of some notoriously hard-to-model separation problems and a description of some of the available simulation software packages.

1 Introduction

Computers are getting cheaper and more powerful every year. At the same time, separation systems are getting smaller and faster. The convergence of these two trends has led to a situation where it is now possible to simulate the key parts of some separation systems at the molecular level. An example of this is the atomistic simulation of the translocation of an ssDNA molecule through a nanopore [1], a process that may lead to the $1000 genome sought by the NIH in the USA.

Transport-based separation systems generally represent a compromise between the physical separation of several molecular species (*e.g.* due to their different velocities in the device) and their spatial spreading due to various diffusion-related processes. Since most separation devices employ sieving, liquids and electric forces, modeling efforts must generally include long-range electrostatic forces, long-range hydrodynamic forces, frictional and diffusion contributions, conformational effects (for macromolecules), entropic factors, gradients of various types, and interactions with surfaces and obstacles. It is the role of the theoretician to reduce the number of factors to a bare minimum in order to design models that can be solved either analytically or numerically. For example, long-ranged hydrodynamic interactions (HI) are often neglected in the case of gel-based separations.

Simulating complex processes using numerical models that include various levels of detail is now widely seen as the third approach to scientific discovery, complementing the well-established experimental and theoretical methods. Computer simulations are more than mere attempts at reproducing experimental results. Because we have full control over the simulation parameters, and because we can measure every conceivable property (including correlations between properties) of a system during a numerical experiment, simulations allow detailed autopsies and diagnostics not normally achievable in a laboratory. They also allow us to explore numerous systems and geometries at relatively low cost.

Historically, several discoveries were first made on a computer, *i.e. in silico*. In the field of electrophoresis, one of us (G.W.S.) and his co-workers [2] first discovered the phenomenon of DNA band inversion using a computer simulation of the biased reptation model [3, 4]. Experiments

Correspondence: Professor Gary W. Slater, Department of Physics, University of Ottawa, 150 Louis-Pasteur, Ottawa, Ontario, Canada K1N 6N5
E-mail: gary.slater@uOttawa.ca
Fax: +1-613-562-5190

Abbreviations: BD, Brownian dynamics; **BFA,** bond-fluctuation algorithm; **DPD,** dissipative particle dynamics; **FENE,** finitely extensible nonlinear elastic; **HI,** hydrodynamic interactions; **LB,** lattice Boltzmann; **LD,** Langevin dynamics; **LJ,** Lennard-Jones; **LMC,** lattice Monte Carlo; **Mbp,** megabase pairs; **MC,** Monte Carlo; **MD,** molecular dynamics; **OMRC,** Ogston–Morris–Rodbard–Chrambach; **SRD,** stochastic rotation dynamics; **WCA,** Weeks–Chandler–Andersen

later confirmed the existence of this counterintuitive phenomenon.

In view of the growing importance of computer simulations in the field of separation methods, we believe that this review is timely. Our hope is that it will be of equal interest to the experimentalist who wants to understand the relevant literature and use simulations to guide his/her laboratory work, to the theoretician who wants to explore novel systems using numerical methods, and finally to the computational scientist who wants to use new tools.

This review article has three main parts. In Section 2, we describe several approaches that are currently being used to model separation processes. We first examine methods that include molecular details, then describe algorithms that simplify the description of the liquid phase, and finish with several coarse-graining methods that generate even simpler numerical models. In Section 3, we review nine well-known problems and the simulation methods that are being used to study them. In Section 4, we look at the future and discuss a few problems that have proven hard to simulate and understand with the current methods. An Appendix then lists some of the most well-known software packages in the field; however, it is important to note that many (perhaps most) simulation studies have actually been based on simulation programs written by the researchers themselves. The choice of material is obviously that of the authors; we recognize that several important algorithms and problems are missing from this review. Among those, approaches based on the continuum description of the flow and the distribution of analytes [5, 6] and reptation models of gel electrophoresis [4, 7–12] are perhaps the most obvious.

2 Simulation methods

In this section we describe some of the most popular simulation techniques used in computational studies of electrophoretic separation methods. It is obviously impossible to review them all – as a matter of fact, new methods are proposed every year. In that light, we present some of the main methods in a way that we believe is both logical (from the more microscopic to the most simplified) and compact. For a more rigorous discussion on levels of coarse-graining see [13]. In our descriptions, we do not strive for the level of detail that would allow readers having no prior knowledge to do their own simulations. Rather, we present a bird's-eye view of the hierarchy of different computational methods. Correspondingly, the number of references is large as the interested reader will need to consult specialized texts in order to fully appreciate the intricacies of these simulation methods.

2.1 Molecular dynamics

The molecular dynamics (MD) technique is used to follow the evolution of a large number of interacting particles by numerically integrating the classical equations of motion. Although MD is often used to simulate systems at the molecular level, it is also suitable for modeling larger-scale systems by implementing coarse-grained methodologies. Hence, it is a common approach to simulating polymer dynamics.

When performing MD simulations, the first step is to calculate the net force on each particle. Newton's second law $\mathbf{F} = m\mathbf{a} = m\ddot{\mathbf{r}}$ then provides the particle's acceleration. Numerically integrating by $\mathbf{v} = \mathbf{v}_0 + \mathbf{a}\Delta t$ yields the particle velocity at a short time Δt later; a second integration $\mathbf{x} = \mathbf{x}_0 + \mathbf{v}\Delta t$ gives its position (in practice, more accurate numerical integration techniques such as the velocity-Verlet algorithm [14, 15] are employed). After performing these calculations for each particle, the new configuration of the system at time $t + \Delta t$ is obtained. This process is repeated to generate trajectories for each particle that, together, comprise a series of snapshots describing the evolution of the system. For conceptual simplicity, we begin by describing a fully atomistic MD simulation (each atom is represented by one particle). However, as this is generally too computationally expensive, we subsequently introduce various techniques to "coarse-grain" the models and make MD a viable tool for studying separation methods. Although we will discuss only a few key topics, there are a great number of excellent books [14–17] and review articles [18–20] that can be used to explore the rich field of MD simulations in greater depth.

2.1.1 The force field

The interactions between the particles in the system obviously play a major role. The mathematical forms and parameters dictating these interactions are known as the "force field"; the key concepts used in this review are discussed below.

2.1.1.1 Lennard-Jones

The interaction between two free, uncharged atoms implies two primary effects. First, there is a short-ranged repulsion preventing overlap. Second, there is a long-range attraction arising from weak but favourable interactions due to induced dipole effects (dispersion forces). The Lennard-Jones (LJ) potential [21] is commonly used to model these effects:

$$U_{\mathrm{LJ}}(r_{ij}) = 4\varepsilon_{ij}\left[\left(\frac{\sigma}{r_{ij}}\right)^{12} - \left(\frac{\sigma}{r_{ij}}\right)^{6}\right] \tag{1}$$

where r_{ij} is the separation between the particles i and j, ε_{ij} is the depth of the potential well and σ is the effective size of the particle (see Fig. 1 for a plot of this potential). The numerical values used for ε and σ dictate the details of the interaction.

2.1.1.2 Coulombic forces

The other primary non-bonded interaction arises from the electrostatic interaction between pairs of particles given by
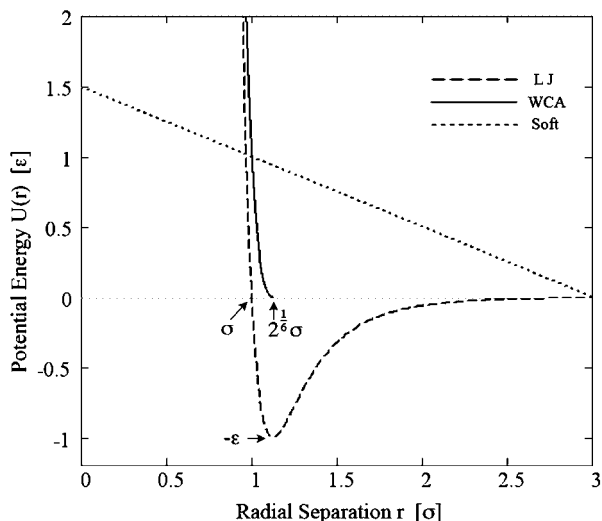
Figure 1. Plot of the full LJ potential, the purely repulsive WCA potential, and the soft potential common in DPD. The positive soft potential of DPD extends far further and avoids the singularity of the LJ and WCA potentials.

the Coulombic potential

$$U_{\mathrm{Coul}}(r_{ij}) = \frac{1}{4\pi\varepsilon_0} \frac{q_i q_j}{\varepsilon r_{ij}}$$

Here, q_i and q_j are the effective charges on each particle, ε_0 is the permittivity of free space, and ε is the dielectric constant of the medium. In atomistic simulations with an explicit, polar solvent model, including ε is not necessary. However, for simulations with either implicit or non-polar solvent models (including the mesoscopic models common in coarse-grained simulations), ε is an effective dielectric constant that includes the screening effects due to the medium (*e.g.* $\varepsilon = 80$ for water). Although the magnitude of the net charge is obvious for free ions, in molecules where charges are shared *via* bonds the value of the effective partial charges is a vital component of the force field. Unlike the LJ interaction that decays relatively quickly, the Coulombic interaction is long ranged. While a cut-off distance (beyond which contributions are not considered) is appropriate in one dimension, the long-ranged contributions are important in two or three dimensions. For this reason, inclusion of electrostatic effects can be computationally expensive and many sophisticated techniques have been developed to address this particular problem. For a review of many of these methods see [22, 23]; further methods are discussed in [24, 25].

2.1.1.3 Bonded interactions

In MD simulations, elements of chemical bonds are captured by implementing potentials to maintain bond lengths and bond angles. Although other forms are used, a common choice for both is a harmonic potential such that the bond stretching $U_{\mathrm{BS}}(r_{ij})$ and bond bending $U_{\mathrm{BB}}(\theta_{ijk})$

potentials are given by

$$U_{\mathrm{BS}}(r_{ij}) = \frac{1}{2} k_{ij}(r_{ij} - r_0)^2 \tag{2}$$

$$U_{\mathrm{BB}}(\theta_{ijk}) = \frac{1}{2} k_{ijk}(\theta_{ijk} - \theta_0)^2 \tag{3}$$

Here, k_{ij} and k_{ijk} are force constants, θ_{ijk} is the angle formed by the bonds joining atoms i, j, k, and r_0 or θ_0 are the equilibrium separation and bond angle respectively. Hence, in this model, atoms are bonded together *via* Hookean springs while the bond angles oscillate around the equilibrium value. In atomistic simulations, the various parameters are an essential part of the force field as they dictate the details of these interactions. Note that while we discuss only bond stretching and bending here, terms can be added to model effects such as restrictions to torsional angles and *cis versus trans* configurations [26].

2.1.2 Coarse graining

A fully atomistic MD simulation is quite detailed in the features it replicates and is appropriate to study dynamics on the nanosecond and nanometer scales. To probe larger systems on longer time scales, the use of coarse-graining techniques is essential.

2.1.2.1 United atoms

The first step in coarse-graining a system is to lump groups of atoms together and simulate them as a single "particle". For example, in atomistic MD simulations of proteins, it is common to group the hydrogens of amino acid side chain carbons in with the carbon to form a united atom. Reducing the number of particles results in reduced computing time while preserving the dynamics of interest. One can extend this idea and model entire side chains (or even entire monomers) as single particles. From this, we can then simulate any polymer as a string of bonded generic beads – each of which represents a monomer. Of course, the interaction between adjacent beads is vital; such local effects can be incorporated by using, *e.g.* a potential between adjacent bonds in the chain to give a finite stiffness to the backbone (for example, the bond angle potential discussed above [27]).

We can extend the level of coarse-graining even further by lumping polymer beads together and simulating *n* monomers as a single particle that now represents a subchain of the polymer. If *n* is large enough such that the length of the subchain is equal to or exceeds the Kuhn length (a measure of the stiffness of the polymer chain), correlations between subchains are negligible and we can simulate the coarse-grained polymer as a freely jointed chain [28]. This is a standard model for studying a polymer *via* MD simulations as it allows for computational simplicity and efficiency while preserving the dynamics of interest. What is lost is the direct correspondence to the system in study and hence an extra layer of abstraction between simulation and reality is introduced.

2.1.2.2 The WCA potential

In coarse-grained simulations, it is common to use the purely repulsive Weeks–Chandler–Andersen (WCA) potential (also known as the truncated LJ potential) to model particle interactions [29]. This is an LJ potential that is shifted and truncated at its minimum value (see Fig. 1) so that it ends smoothly at a distance $r_c = 2^{1/6}\sigma$:

$$U_{\mathrm{WCA}}(r_{ij}) = \begin{cases} 4\varepsilon_{ij}\left[\left(\frac{\sigma}{r_{ij}}\right)^{12} - \left(\frac{\sigma}{r_{ij}}\right)^{6}\right] + \varepsilon_{ij} & \text{for } r_{ij} < r_c \\ 0 & \text{for } r_{ij} \geq r_c \end{cases} \quad (4)$$

However, the standard LJ interaction is often used to study systems with varying affinities between different types of particles (this is implemented by varying the ε_{ij}'s).

2.1.2.3 Finitely extensible bonds

In a coarse-grained model, the use of harmonic potentials to connect adjacent beads can lead to unphysical bond stretching effects. For this reason, a finitely extensible force is needed such that there is a hard limit on the bond length. The most common choice is the finitely extensible nonlinear elastic (FENE) potential:

$$U_{\mathrm{FENE}} = -\frac{1}{2} k r_0^2 \ln\left(1 - \frac{r^2}{r_0^2}\right) \quad (5)$$

Here, k indicates the stiffness of the bond and r_0 gives the maximum bond length (the potential shoots to infinity as r approaches r_0). For appropriate values of k and r_0, the occurrence of ''bond crossing'' is extremely rare and hence behaviour appropriate for a self-avoiding polymer is produced [30]. It is interesting to note that this form is an approximate solution to the inverse Langevin function; in some cases, it may thus account for the entropic restoring force, which arises from stretching a subchain [28].

2.1.3 Simulating a polymer

Putting the above together, the simplest model of a polymer in a coarse-grained simulation is a freely jointed chain of beads (which can either carry a net charge or be neutral) interacting by the WCA potential (or the LJ potential when short range attractions are desired) and with immediately neighbouring monomers bonded *via* the FENE potential. Extension to branched polymers is trivial. Although we have sacrificed many details, we have preserved effects such as excluded volume, the entropic elasticity, and the noncrossability of bonds. Although this model may seem very crude, it does allow for a realistic scaling behaviour of polymeric properties such as the radius of gyration and the diffusion coefficient with respect to the degree of polymerization. This approach also represents the most realistic model of polymers for which experimentally relevant simulations are feasible. Note that although this ''bead–spring'' model is a common approach, other models can be employed. For example, algorithms can be implemented to

maintain the bond distance at a fixed length [31, 32] resulting in a ''bead-rod'' model (or a ''pearl-necklace'' model for the case of the rod length being comparable to the diameter of the bead) [33].

Now that we have a model for the polymer, we can add other components. For example, a common scenario involves simulation of polyelectrolytes with free ions. To accomplish this, ions can be defined as WCA particles carrying a net charge. Additionally, one can include features such as obstacles or boundaries (*e.g.* walls) by building them out of particles or defining them using mathematical constraints. The final, and critical, component of the simulation system is the solvent. As the model used for the fluid impacts both the dynamics that are observed and the computational time, Sections 2.2–2.4 will focus on various ways of treating the fluid.

At this point, it is important to mention that choosing a method of controlling the temperature is often a crucial consideration in MD simulations; in fact, it is also one that is often intimately connected to the choice of solvent model. Implementing a thermostat is particularly critical when an external field is adding energy to the system – as in electrophoresis. Although there are schemes based on rescaling the velocities [34] or periodically assigning random velocities [35], such algorithms can lead to artefacts as local momentum is not conserved (a particular problem when hydrodynamics are of interest [36]). In coarse-grained simulations, the method chosen for treating the fluid often involves a particular temperature control scheme *via* the coupling of the analyte (*e.g.* the polyelectrolyte) to the fluid. An important case is the thermostat developed for dissipative particle dynamics (DPD) (Section 2.3.1), which can be used independently of the fluid model and, for several reasons, has been a significant advancement in the field [37]. Finally, in the case of performing Langevin dynamics (LD) or Brownian dynamics (BD), the temperature is explicitly in the equation of motion (Section 2.4). Although discussing the details of these algorithms (and others [38–41]) is beyond the scope of this review, the interested reader is encouraged to investigate these various schemes starting with the citations given and the discussion of solvent models in the following sections.

2.2. Explicit fluid

At the atomistic level, many models exist that explicitly describe a water molecule [42–45]. In fact, developing appropriate models for simulating water alone is the subject of active research. In coarse-grained simulations of solvents, we group atoms, and even molecules, together and simulate them as a single bead. The use of the WCA potential for this solution of beads is found to provide a good solvent, regardless of temperature [46]. The advantage of using an explicit fluid is that it is conceptually obvious and preserves the long-range HI that correlate the movement of objects in a fluid. However, in practice, this results in much of the simulation time being dedicated to calculating the details of

the fluid bead dynamics, which are often not of interest. For these reasons, several techniques for modeling the fluid to maintain the HI while neglecting the computationally costly details of the fluid motion have been developed. These models are discussed in the following section.

2.3 Mesoscopic fluid

It is possible to describe hydrodynamic effects without resorting to an explicit description of fluid molecules or the discretization of the continuous Navier–Stokes equations. In particular, a clever use of conservation laws allows mesoscopic methods to employ local algorithms that recover the solution to the hydrodynamics equations in the large-scale/long-time limit while at the same time bypassing the molecular details of the fluid and thus dramatically reducing the computational cost of the simulation. In the following sections we will review three mesoscopic approaches, namely DPD, stochastic rotation dynamics (SRD) and lattice Boltzmann (LB).

Following the description of these mesoscopic methods, Section 2.4 will introduce LD and BD. A comparison of the different methods discussed ensues in Section 2.5 where a schematic is presented to summarize each of the methods.

2.3.1 Dissipative particle dynamics

In DPD, the fluid is modelled by large particles interacting *via* a *soft* potential [47–49]. This allows for a reduction in computing time in two ways. First, as each DPD fluid bead represents a cluster of fluid molecules moving together in a coherent manner, the simulation tracks a much lower number of interacting objects. Second, since with a soft potential the forces cannot be arbitrarily large, we can reduce computing times by increasing the integration time step. All particles interact by three forces: a conservative force $\mathbf{F}^C$, a dissipative force $\mathbf{F}^D$, and a random force $\mathbf{F}^R$:

$$\mathbf{F}_i = \sum_{i \neq j} \left(\mathbf{F}_{ij}^C + \mathbf{F}_{ij}^D + \mathbf{F}_{ij}^R \right) \tag{6}$$

where it is assumed that the interactions are negligible beyond a cut-off radius r_c. Pairwise potentials ensure that momentum and angular momentum are conserved. The force $\mathbf{F}_{ij}^C$ represents and can include any conservative forces that act on the particle. A common choice is a soft repulsion (see Fig. 1) acting along the line of centres such as

$$\mathbf{F}_{ij}^C = \begin{cases} a_{ij}(r_c - r_{ij})\hat{\mathbf{r}}_{ij} & \text{for } r_{ij} < r_c \\ 0 & \text{for } r_{ij} \geq r_c \end{cases} \tag{7}$$

where a_{ij} parametrizes the maximum repulsion. The dissipative force is an inter-drag force between a pair of soft fluid particles moving through each other opposing their relative motion $\mathbf{u}_{ij}$ and dissipating heat:

$$\mathbf{F}_{ij}^D = -\omega^D(r_{ij})\zeta(\hat{\mathbf{r}}_{ij} \cdot \mathbf{u}_{ij})\hat{\mathbf{r}}_{ij} \tag{8}$$

where ζ is the friction constant between the two clusters. The random noise force is given by

$$\mathbf{F}_{ij}^R = \omega^R(r_{ij})\sqrt{2\zeta k_B T}\frac{\gamma_{ij}}{\sqrt{\Delta t}}\hat{\mathbf{r}}_{ij} \tag{9}$$

where γ_{ij} is a random number of zero mean and unit standard deviation. To satisfy the fluctuation–dissipation theorem, the dissipative and random forces are interrelated through the weight functions, as $\omega^D(r) = [\omega^R(r)]^2$.

The random and dissipative forces act as a source and a sink for heat, respectively. Therefore, DPD, unlike BD or LD is an implicit thermostat [37, 50] that conserves linear and angular momentum and thus recovers hydrodynamics in the macroscopic limit. It should be noted that DPD does not conserve total energy, but only mass and momentum. Solutes can be included as DPD beads and by the inclusion of a bead–spring type force in Eq. (6), DPD can simulate polymers as well [50, 51]. In fact, DPD can be used as an effective thermostat that conserves HI, independently of the fluid model [37].

2.3.2 Stochastic rotation dynamics

The DPD beads represent clusters of many particles but all bead–bead interactions must still be evaluated. In SRD [52–54], also called multiparticle collision dynamics [55, 56] or real-coded lattice gas [57, 58], collisions between fluid particles are replaced by multiparticle collision events that omit the molecular details and eliminate the need to calculate the forces between the fluid particles. These events are defined to conserve mass, momentum, and energy such that the hydrodynamic equations of motion are obeyed on sufficiently long length and time scales [59]. SRD simulations occur in two steps. During the first, or *streaming*, step, the particles move ballistically, and their positions $\mathbf{r}_i(t)$ are updated in discrete time intervals δt:

$$\mathbf{r}_i(t + \delta t) = \mathbf{r}_i(t) + \mathbf{v}_i(t)\delta t \tag{10}$$

The second, or collision, step transfers momentum between particles. The simulation domain is partitioned into cells. The number of particles in each cell may vary from one cell to another but the total number is conserved. Each cell has a centre of mass velocity $\mathbf{v}_{CM}$, which corresponds to the local macroscopic velocity. The collision step is a simple nonphysical scheme that is constructed to conserve momentum. Multiparticle collisions within each cell are represented by the operation

$$\mathbf{v}_i(t + \delta t) = \mathbf{v}_{CM}(t) + \mathbf{R}(\mathbf{v}_i(t) - \mathbf{v}_{CM}(t)) \tag{11}$$

By making the collision operator, $\mathbf{R}$, a rotation through an angle α about a randomly chosen axis, conservation of energy, isotropy and a Maxwell–Boltzmann velocity distribution are met in the continuum limit. Other choices allow SRD to operate as a thermostat as well [60]. Unfortunately, Galilean invariance is broken by the discretization of space into cells. However, this can be completely remedied by performing the collision operation in a cell grid, which is shifted each time step by a random vector [61, 62].

When integrating SRD into a standard MD simulation the solute particles can be coupled to the momentum of the fluid by including them in the SRD collision step (Eq. 11) [55, 56, 63–65]. In typical simulations of a polymer, on the order of 10^2 MD time steps are performed between SRD collision events [54, 66–68]. This separation of time scales ensures that the momentum transferred to the polymer during the collision step is well distributed throughout the chain [69]. Another common scheme uses a hybrid SRD/MD approach in which not only the solute–solute but also the solute–solvent interactions are handled by an MD algorithm, while solvent–solvent interaction is simulated by SRD [53, 70, 71].

2.3.3 Lattice Boltzmann method

LB coarse-grained models [54, 72, 73] are based on a solution of the discretized Boltzmann transport equation. The main quantity in the LB approach is the velocity field, rather than fluid particles, and it is an inherently statistical approach, where discrete momentum distributions are represented on a spatial grid.

The discretization of positions and momenta using finite sets of directions greatly simplifies the problem. The most frequent mesh types for the LB simulations are the D2Q9, D3Q15, and D3Q19 lattices, where DkQn refers to the number k of dimensions and to the discrete number n of velocity vectors, $\mathbf{e}_i$.

A set of distribution functions $\Gamma_i(\mathbf{r}, t)$ is defined on each lattice site $\mathbf{r}$. Each of these can be interpreted as the fraction of fluid that will move with the ith discretized velocity at time t. The discretized Boltzmann equation provides a generic description for the time evolution of the probability density, but there is freedom in the choice for the actual form of the collision integral. A common formulation is the Bhatnagar–Gross–Krook approximation, where

$$\Gamma_i(\mathbf{r} + \mathbf{e}_i\Delta t, t + \Delta t) = \Gamma_i(\mathbf{r}, t) - \frac{\Delta t}{\tau}(\Gamma_i(\mathbf{r}, t) - \Gamma_i^{EQ}(\mathbf{r}, t)) \tag{12}$$

where τ is the phenomenological relaxation time, which prescribes the timescale for the relaxation of the actual population Γ_i to the equilibrium particle distribution function Γ_i^{EQ}. In the low velocity approximation, Γ_i^{EQ} can be expressed as

$$\Gamma_i^{EQ} = w_i\rho\left[1 + \frac{\mathbf{e}_i \cdot \mathbf{u}}{c_s^2} + \frac{(\mathbf{e}_i \cdot \mathbf{u})^2}{2c_s^4} - \frac{u^2}{2c_s^2}\right] \tag{13}$$

where ρ is the hydrodynamic density and c_s is the speed of sound, which is determined by mesh properties. The weights, w_i, must be suitably chosen to recover the macroscopic Navier–Stokes equations and are dependent on the mesh configuration [54]. The viscosity of the LB fluid is determined by the choice of the relaxation rate.

LB can be coupled to small suspended spheres by treating them as point particles that interact with the fluid through a friction force proportional to the relative velocity obtained *via* linear interpolation from the surrounding lattice sites [74, 75]. By adding fluctuation terms to both the fluid and the embedded particles, LB can operate as an adequate thermostat [74]. The correct treatment of a fluctuating LB algorithm has been recently addressed in several papers [76, 77].

2.4 Langevin and Brownian dynamics

Going beyond mesoscopic models, further coarse graining can be achieved by avoiding direct simulation of the fluid altogether. The timescale of individual collisions with solvent molecules (causing frictional drag and Brownian motion) is much smaller than the time scales relevant to electrophoresis. It is computationally advantageous to coarse grain out the fine details of the collisions and simply include their statistical effect on the solute. One may consider implicitly the two main effects of the fluid acting on the particle: (i) a frictional force opposing its motion and (ii) random kicks arising from collisions with the solvent. The frictional (or dissipative) force $\mathbf{F}^D(t)$ removes energy from the particle while the fluctuating Brownian force $\mathbf{F}^B(t)$ adds energy to the particle. Hence, at this coarse-grained level, the fluid is included solely in a statistical manner governed by the fluctuation-dissipation theorem. By replacing the explicit fluid with a drag and a Brownian force, we lose the long-range particle–particle interactions mediated by the fluid. This makes such an approach particularly tempting when the HI are negligible or not of primary concern. Nevertheless, we will see how they can still be included.

2.4.1 Pure Langevin and Brownian dynamics

In LDs, starting with Newton's second law as we did for pure MD, we now add a dissipative drag force $\mathbf{F}^D(t)$ and a Brownian force $\mathbf{F}^B(t)$ (in addition to the conservative forces we had before, $\mathbf{F}^C(t)$) to end up with Langevin's equation

$$m\mathbf{a}(t) = m\ddot{\mathbf{r}}(t) = \mathbf{F}^C(t) + \mathbf{F}^D(t) + \mathbf{F}^B(t) \tag{14}$$

where m is the mass of the particle. For the dissipative term, one usually assumes Stokesian drag on a spherical particle, $\mathbf{F}^D(t) = -\zeta\mathbf{v}(t)$, ζ being the friction coefficient of the particle in the fluid. The velocity $\mathbf{v}(t)$ is then the velocity of the particle with respect to the local solvent velocity. This is an important detail if one wants to consider flow or long-range HI. Although $\mathbf{F}^B(t)$ is due to the solvent molecules colliding with the particle, it can only model the net effect of a large number of collisions. The Brownian force is taken as a centred Gaussian random variable [78] with zero mean and variance $2\zeta k_B T/\Delta t$, where Δt is the integration time step. The fact that the variance is related to the friction coefficient ζ is again a consequence of the fluctuation–dissipation theorem. On the time scale of

interest the values of the Brownian force are uncorrelated at different time steps.

It can be shown that the energy transferred to the particle from a single collision with a solvent molecule decays on the viscous time scale m/ζ [79]. If, as is typically the case, this is much smaller than the timescale over which $\mathbf{F}^C(t)$ changes (overdamped limit), we may set $m\mathbf{a}(t) = 0$ in the Langevin equation and obtain the following discretized equation of motion:

$$\mathbf{r}(t + \Delta t) = \mathbf{r}(t) + \frac{\Delta t}{\zeta}[\mathbf{F}^B(t) + \mathbf{F}^C(t)] \qquad (15)$$

which defines BD. For a more rigorous derivation see [80].

2.4.2 Incorporating long-range hydrodynamic interactions

Traditionally, LD does not include HI between particles. This approximation is valid for certain systems (*e.g.* when HI are screened out), but in many cases HI have a significant impact on the dynamics [81].

To see how we can incorporate them, let us consider a particle *i*. As it is moving with a certain velocity, it slows down due to the drag force. Since the drag force exerted by the fluid on a particle must be equal and opposite in direction to the force exerted by the particle on the fluid, this causes the fluid to move. Hence, the effect particle *i* has on particle *j* is that the latter experiences a modified drag as it is no longer surrounded by a stationary fluid. The magnitude of this coupling depends on their relative separations. On the time scale of interest this perturbation can generally be considered to be felt instantaneously. In a many-particle system, a common approximation is to ignore screening issues and to consider a superposition of all pairwise HI [82].

Consideration of the fluctuation–dissipation theorem implies that any modulation of the drag term must be accompanied by correctly modifying the magnitude of the Brownian term. An interesting consequence is the correlation of the Brownian forces on different particles at the same time. In practice, the relationship between the drag and the Brownian term is determined *via* interaction tensors (mainly the Oseen or Rotne–Prager–Yamakawa tensor). Application details can be found in [79, 80, 82–87].

2.5 Comparison of fluid models

We have presented a hierarchy of fluid models from the most detailed explicit solvent models to the mesoscopic and, finally, implicit (LD and BD) approaches. Using explicit models (especially the atomistic variant) is essential when high accuracy and the chemical details (such as different hydrophobicities of different parts of the analyte) are required. In most other cases, simpler approaches should be used. All three mesoscopic methods (DPD, SRD, and LB) use a simple (but often sufficient)

model to describe fluid dynamics and can also act as thermostats that define the local temperature when coupled to MD particles.

Owing to their conceptual differences, these methods use different types of parameters to describe the fluid, which results in a different suitability for specific problems. For example, while the fluid viscosity is directly accessible in LB methods, it becomes a combination of different parameters and can be controlled only indirectly in DPD [88, 89]. Similarly, while DPD and LB can only approximate the continuous-time dynamics of the fluid when the discrete time step is small, SRD is proven to yield correct long-time hydrodynamics for any step size. However, SRD's transport properties depend explicitly on the chosen time step [59]. More differences between the methods arise if confined fluids or interactions with large obstacles or particles are studied. Here, the ability to treat different boundary conditions becomes important, which is covered in detail in the literature [53, 63, 90–94].

All three methods share a similar computational efficiency, and computation times depend mainly on the implementation, the computer system, and also the investigated system. However, the speedup over explicit fluid simulations can be a factor 20 or higher [74, 95].

These mesoscopic models describe compressible fluids in which hydrodynamic forces need time to propagate through the medium. For this reason, as well as considerations of computational speed, performing LD with proper inclusion of HI can be preferable in some cases [96]. Furthermore, if the full treatment of HI is not necessary, the use of pure LD or BD is advisable.

We summarize the different ways of treating the solvent in MD simulations with a schematic that depicts the most important features of different fluid models (Fig. 2).

2.6 Monte Carlo simulations

In addition to the coarse-graining introduced previously, it is reasonable to ask whether it is possible to also coarse-grain the dynamics itself in order to achieve further computational speedup. This is the motivation behind the development of the various Monte Carlo (MC) methods.

In the broadest sense of the term, any computational method involving randomness can be called an MC method (the name says it all!). This broad definition would, however, include, *e.g.* BD, already considered under the banner of MD. In the spirit of the preceding discussion, we would therefore call an MC method any approach that sacrifices at least some of the dynamical details of the MD methods. How much is sacrificed can vary. At one extreme are methods designed to study equilibrium properties by quickly exploring large parts of the phase space. In this case, unphysical moves, such as rotations of large parts of chains in the pivot algorithm [98], can be introduced on purpose to speed up the simulation. Since in simulations of electrophoresis and related separation methods we are primarily interested in the dynamics of the
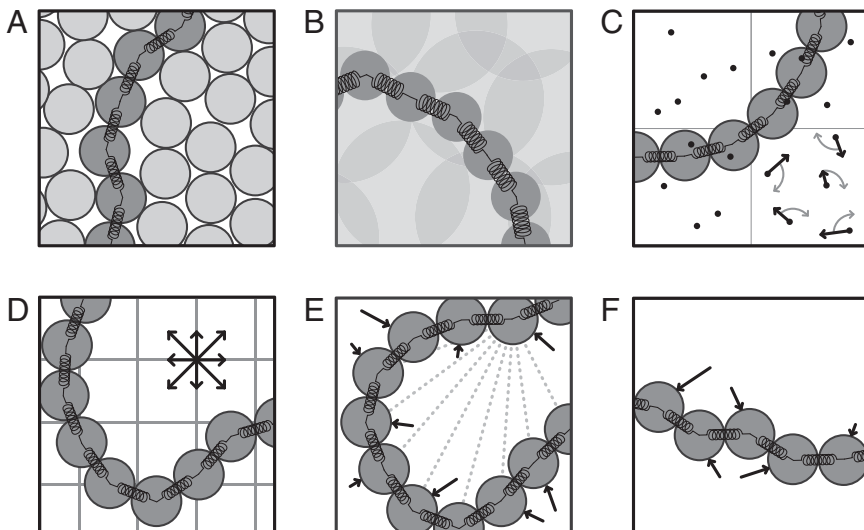
Figure 2. Schematic depicting different methods of modeling the solvent in MD simulations. In each case, a representative polymer is shown as a chain of beads connected by springs. (A) The explicit fluid approach models the solvent as beads interacting through a short-range potential and simulated to the same level of detail as the polymer. Fluid particles are often chosen to be the same size as the monomers. (B) The DPD method typically models the solvent as large, overlapping, softly repulsive spheres. (C) The SRD method replaces collisions between particles by a multiparticle collision operator, which models the local collisions as a rotation of particle velocity through an angle about a randomly chosen axis. (D) In LB the fluid is discretized to a grid. Arrows symbolize the discrete set of allowed velocities. The mesh shown is a D2Q9 (eight velocity vectors plus the zero velocity in two dimensions). (E) LD/BD represents the fluid implicitly by including a friction and a random term in the equation of motion of each monomer. HI can be included by introducing an additional long-range force between monomers (illustrated for one bead as a series of dashed lines). (F) Pure LD/BD neglects HI — friction and Brownian forces are the only effects of the solvent that are included. After Padding and Louis [97].

analytes, such MC approaches are less useful for our purposes, although they can be applied to some auxiliary problems, such as generating an equilibrated entangled sieving polymer solution in which the analytes would then migrate, studying the properties of capillary coatings, or finding the free energy of a DNA molecule as a function of its coordinate along a nanopore. We do not discuss these methods here; they are reviewed, *e.g.* in [99–101]. Instead, we concentrate on dynamical MC algorithms.

MC methods can be divided into two groups. In off-lattice MC methods, particles and monomers of polymer chains can occupy any positions in space. But one can also discretize the space allowing the particles to reside only at the nodes of a lattice. Such methods are known as Lattice MC (LMC). Since the sets of possible configurations and moves are then discrete, they can be described using integer arithmetic and often special computational techniques, such as multispin coding ([102], Section 15), which allow significant savings in computer time and memory compared with off-lattice MC. Of course, the cost of increased efficiency in LMC is even less realism!

Our ideal goal when simulating electrophoresis problems is to make quantitative predictions for the mobility and diffusivity of the analyte. Although this is possible in simple cases, MC simulations are generally used to predict trends (including scaling laws) and qualitative features, which in many cases is quite acceptable.

We start our discussion of MC methods with approaches to simulating hard particles. We then discuss some chain simulation methods. As discussed in Section 1, we will not describe the MC methods used to simulate DNA reptation models [103].

2.6.1 Methods for particles

Consider a particle undergoing Brownian motion in the presence of an external force (*e.g.* an electric field) and some obstacles (*e.g.* gel fibres). In MC, this becomes a simple biased random walk. At each time step, a move is randomly selected from a predefined set, and a test is used to accept or reject it. A simulation is simply a series of such moves. Different MC algorithms are defined by: (i) the set of moves and the probability of selecting a particular move from that set; (ii) the acceptance test for the selected move; and (iii) the time step *per* move. Although the physics behind these three elements can be subtle (the main issue is generally the definition of the time scale), the simulation itself is often quite simple.

The most popular MC approach is Metropolis MC [104], a method designed to study equilibrium configurations. In the simplest lattice variant, at each step the particle simply tries to move to any of the neighbouring sites on the lattice, and all possible moves can be selected with equal probability. Moves can be accepted or rejected. If the change in energy from the initial to the final configuration is negative ($\Delta U < 0$), the move is accepted; otherwise, it is accepted with probability $\exp(-\Delta U/k_B T)$ (the Boltzmann factor). If the move is rejected, the particle remains in its previous

position, but the clock is still advanced by one unit of time. This is known as the Metropolis test. The latter guarantees that the correct equilibrium properties are obtained. However, reproducing the correct dynamics is problematic. First of all, how the MC unit of time (an attempted move) is related to actual time is usually left undefined, which makes quantitative predictions difficult. Moreover, in a high field the method is even qualitatively wrong: once $|\Delta U|/k_B T \gg 1$, all steps along the field are accepted and all those against the field are rejected; as a result, the velocity saturates and the diffusion coefficient vanishes. A different approach is then required.

In the 2-D lattice variant of such an approach [105], the system is modelled as a square lattice, where each node is either free or is an impenetrable obstacle. At each time step, the particle can move in one of four directions ($\pm\hat{x}, \pm\hat{y}$). Unlike in the Metropolis algorithm, the probabilities of selecting each of these moves are no longer equal; instead, if an external force $\vec{F} = F\hat{x}$ is applied to the particle, they are given by [105]

$$p_{\pm x}(\varepsilon) = \frac{1}{(1 + e^{\mp 2\varepsilon})(1 + \tanh(\varepsilon)/\varepsilon)}$$

$$p_{\perp}(\varepsilon) = \frac{1}{2(1 + \varepsilon \coth(\varepsilon))} \tag{16}$$

where the scaled force ε is given by

$$\varepsilon = \frac{Fa}{2k_B T} \tag{17}$$

with a the mesh size of the lattice. Note that the algorithm is rejection-free in the absence of obstacles; however, moves leading to an overlap between the particle and an obstacle are rejected. The time step is no longer arbitrary as it is given by the expression

$$\tau(\varepsilon) = \frac{\tau_B}{1 + \varepsilon \coth(\varepsilon)} \tag{18}$$

where $\tau_B \equiv \tau(\varepsilon = 0)$ is the mean duration of a (Brownian) jump in the absence of an external field. The latter is directly related to the free-space diffusion coefficient D_0:

$$\tau_B = \frac{a^2}{2D_0} \tag{19}$$

It is this relation that connects the MC and experimental times. The above choice of transition probabilities and the time step can be shown [105] to give the correct average velocities for fields of arbitrary strength. However, the dispersion coefficient is correct only in the limit of a vanishingly small field [106]. In this limit, the dispersion coefficient D can actually be obtained more efficiently by using the Nernst–Einstein relation:

$$D = \lim_{F \to 0} k_B T \mu(F) \tag{20}$$

where $\mu(F) = v(F)/F$ is the mobility. In a non-vanishing field, the correct dispersion coefficient can be obtained by varying the time step (making it a random number) [106]. If a constant time step is desired (as is the case for the

numerically exact algorithm that we describe next), the MC moves themselves must be modified [106, 107].

2.6.1.1 Exact calculation method

Standard MC methods require a large amount of simulation data in order to have a low statistical error. In recent years, our group has developed a numerical method that allows one to compute the exact mean velocity and diffusion coefficient of a particle moving on a lattice with impenetrable obstacles. This method, which basically gives the exact solution to the MC simulation, is both faster and more precise. We now show the basics of this approach. For further details, the reader can refer to [108, 109].

The first step is to obtain the transition matrix T whose elements T_{ij} are probabilities that a particle on site j jumps to site i in a single time step. If at time t, the probability of presence of the particle on site i is $n_i(t)$, then after a single time step,

$$n_i(t + \tau) = \sum_j T_{ij} n_j(t) \tag{21}$$

Implicitly, this assumes that the time step is unique; since the latter depends on the field intensity, the method works only in a uniform field (unless the field is so weak that the field dependence of $\tau(\varepsilon)$ can be neglected). The steady state, defined by the equality $n_i(t + \tau) = n_i(t) \equiv n_i$, is thus the normalized eigenvector of T with the eigenvalue of unity (the normalization condition is $\sum_i n_i = 1$). This eigenvector, which can be obtained with an arbitrary precision by a simple numerical calculation, is the exact solution of the LMC algorithm.

Once the steady-state occupation probabilities $n_i(\varepsilon)$ are computed, the mean velocity of the particle, $v(\varepsilon)$, can be obtained by averaging over all sites, $v(\varepsilon) = \sum_i n_i(\varepsilon) v_i(\varepsilon)$, where the average *local* velocity on site i is

$$v_i(\varepsilon) = \frac{p_{+x}(\varepsilon) L_+(i) - p_{-x}(\varepsilon) L_-(i)}{\tau(\varepsilon)} \tag{22}$$

with the displacements $L_{\pm} = a$ if there is no obstacle in the given direction and zero otherwise.

The dispersion coefficient D in the zero-field limit can be calculated using Eq. (20). In a non-vanishing field, D can be obtained with a numerically exact method based on the generalized Taylor–Aris dispersion theory [110].

2.6.2 Methods for chains

Simulating polymer chains presents additional challenges since connectivity and (often) non-crossability of chains have to be maintained during the simulation. In MC simulations of polymer chain dynamics, only one monomer (or, at most, a small local group of monomers) is moved at each step. This choice is necessary in order to keep the frequency of moves leading to overlaps sufficiently low. However, a unit of time should now correspond to one attempted move per monomer.

2.6.2.1 Off-lattice methods

In the most straightforward and commonly used off-lattice MC method for bead–spring chains [111], a single step consists in displacing a monomer chosen at random along each axis, by an amount chosen from the uniform distribution on $[-\Delta/2, +\Delta/2]$, where Δ is a predefined constant. The event is accepted or rejected according to the Metropolis criterion, but all attempts make the clock advance. If the arbitrary parameter Δ is too small, the evolution of the system may be too slow; if Δ is too large, the rejection rate is too high. The optimal Δ normally corresponds to an acceptance rate of about 50%, although a lower Δ can make the dynamics more realistic. The same potentials as for MD (*e.g.* the FENE and WCA potentials) can be used. Besides this, one can use much simpler potentials, such as a square-well bond potential that is zero within a specified range and infinity outside, with the range chosen (just as in FENE) to avoid chain crossings. This improves the efficiency as the computation of complicated potential functions is avoided. However, in this case the chain will have no tension and so square-well potentials should be avoided in strong fields (see below).

In the bead–rod model [112], the bond lengths have to be preserved explicitly. The simplest moves are then rotations of a monomer around the axis connecting its two neighbours (for an end monomer, the rotation is on the sphere with the centre at its neighbour). Note, though, that in a strong electric field, when the chain is stretched, such moves are rather inefficient and this may lead to unphysical artefacts.

2.6.2.2 Bond-length-preserving lattice methods

In lattice models of polymers, monomers still hop between lattice sites, like in single-particle models. To avoid introducing a bond potential and still make sure that neighbouring monomers remain close in space, only those motions that keep all bond lengths within a certain range are allowed. The first models were particularly restrictive in this respect, keeping all bond lengths strictly fixed. Verdier and Stockmayer [113] have used a simple cubic lattice requiring the polymer bonds to coincide with the lattice bonds and thus making them all of unit length. In the first version of the model, only single-monomer motions were allowed. This was later found too restrictive and various two-monomer motions were added, the most popular of which is the so-called crankshaft motion [114]. Unfortunately, the dynamics in such models become very slow if we introduce excluded volume interactions by forbidding two monomers to reside on the same site. Moreover, Madras and Sokal [115] showed that for *any* model with *any* finite set of moves where neighbours along the chain remain neighbours on the lattice some configurations cannot be reached (*i.e.* the algorithm is non-ergodic). Nevertheless, in those cases where excluded volume interactions can be neglected, the Verdier–Stockmayer and other similar approaches can still be useful.

2.6.2.3 Bond-fluctuation algorithm

The deficiencies of the fixed bond length MC models led to the development of lattice methods with fluctuating bond lengths. The most popular one is the bond-fluctuation algorithm (BFA) first proposed by Carmesin and Kremer for 2-D problems [116] involving both linear and branched polymers. Although BFA is not strictly ergodic, its non-ergodicity problems can probably be neglected for all practical purposes. The algorithm was extended to 3-D by Deutsch and Binder [117].

In the BFA (Fig. 3), the monomer is represented by a 2×2 square (four lattice sites) in 2-D and a $2 \times 2 \times 2$ cube (eight lattice sites) in 3-D. A lattice site can be occupied by only one particle at a time. In 2-D, the bond lengths between connected monomers must be less than 4, while in 3-D bond lengths must be $\leq \sqrt{10}$, excluding $\sqrt{8}$. These simple conditions allow for a self-avoiding walk in which there is no crossing of bonds. Each attempted move consists of first picking a monomer at random and moving it by one lattice site along one of the lattice axes. As long as the new conformation does not create monomer overlaps or create a forbidden bond length the move is accepted. As before, a unit time corresponds to one attempted move *per* monomer.

For simulations of electrophoresis, obstacles can be placed at some lattice sites and the field is treated as in other models, by using the Metropolis test. In principle, other interactions, such as intra- and interchain interactions between monomers, can be included as well, but in most cases this is unnecessary (an exception is for the proper modeling of polymer stiffness, an important factor for DNA simulations).
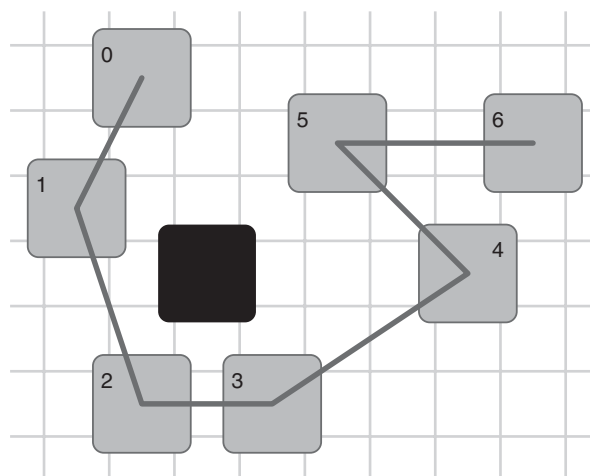
Figure 3. A polymer chain in the 2-D BFA. Each gray square represents a monomer occupying 2×2 sites. All allowed bond lengths from 2 (between monomers 2 and 3) to $\sqrt{13}$ (between monomers 3 and 4) are present in this figure. Allowing only these bond lengths and forbidding the monomers to overlap with the obstacle (black) is sufficient to ensure that the chain does not pass through the obstacle and does not cross itself. After Ref. [118]

2.6.2.4 Problems in strong fields

LMC models considered here have severe problems in strong electric fields. For instance, in gel electrophoresis simulations, the speed of the polymer decays exponentially as a function of the field, while experimentally, the electrophoretic mobility is essentially field-independent in the strong-field limit. To understand the reasons for this failure, consider a chain hooked upon a post with the two unequal arms pointing along the field and sliding off the post [119]. The sliding time is inversely proportional to the field intensity. But in LMC, since only local moves (*e.g.* single-monomer moves) are allowed, the only way for the chain to move is *via* chain slacks originating at the end of the short arm and propagating against the field. The probability for the slack to go all the way to the post decays exponentially with the potential energy difference between the tip of the arm and the post. If the short arm of the hooked conformation is of length L_s, the mean time between successful events will thus increase roughly like $\exp(+FL_s/kT)$, where F is the force on the monomer. This increase being an artefact of the model (the tension does not propagate along the backbone), the model can work only if the argument of this Boltzmann factor is much smaller than unity. Since L_s is proportional to the number of monomers in the chain, N, the maximum allowed external force scales like $F \propto N^{-1}$. This is too restrictive to be useful in practice. In order to solve this problem, one must modify the lattice models by adding *non-local moves*, an idea first implemented by Deutsch and Reger [119] and Duke and Viovy [11] for reptation models. Azuma and Takayama [120] added such moves to the BFA. Although their approach is not very carefully justified, it produces qualitatively reasonable results.

2.6.2.5 Numerically exact methods for chains

LMC algorithms for chains can sometimes be solved exactly, similar to how this is done for single particles. This was done by Boileau and Slater [121] for the BFA. The major complication is that each possible chain conformation and location should be considered a separate state and the number of such conformations grows exponentially with the chain length. For this reason, the approach is only practical for very short polymers (linear or branched). Of course, the solutions are only exact for the dynamics of specific algorithms, which are themselves approximate. We should also mention a numerically exact solution of the MC approach to studying polymer translocation through nanopores [122] that reduced this problem to a 1-D biased random walk by using a calculated dependence of the entropy of the chain on the number of monomers that have passed through the nanopore.

3 Simulation examples

In this section, we discuss nine current problems in the fields of separation science and electrophoresis. We examine

the systems by focusing on the type of simulation methods that are being used to study them. The choice of a numerical model is directly related to the question being asked. For example, coarse-grained methods are ideal for generic investigations of the basic mechanisms leading to separation while microscopic methods may be required when more specific problems are to be solved. To give the reader a broad view of the importance of simulations in our field, we have selected a wide range of problems.

3.1 EOF

EOF is ubiquitous in electrophoresis. EOF occurs when there is an electric field with a tangential component at a charged surface in contact with a liquid. The mobile counterions that make up the Debye layer next to the surface viscously drag the rest of the fluid. Although it is sometimes possible to solve for the fluid velocity profile analytically [123], computational modeling is often used to garner a better understanding of EOF. Let us examine the simple example shown in Fig. 4 where we can see the results of some MD simulations, which are described in detail by Tessier and Slater [124]. The solid line shows the net charge distribution, which has a maximum next to the wall followed by an
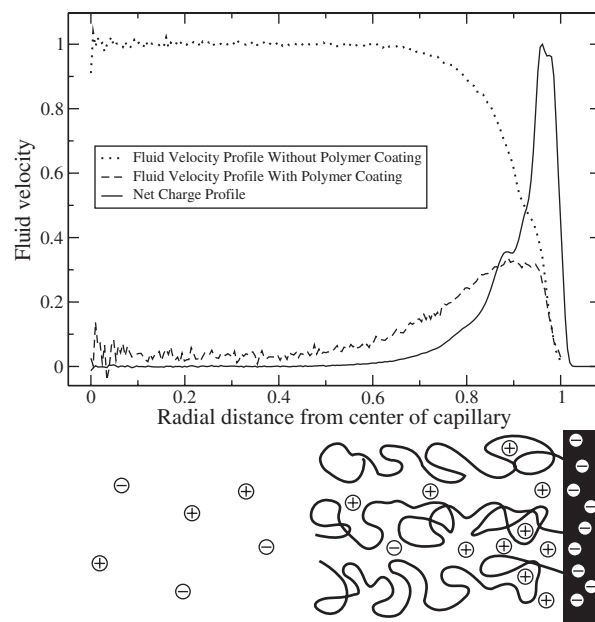
Figure 4. The radial profiles of the fluid velocity from MD simulations with and without a polymer coating, as well as the net charge density profile. The fluid velocities have been normalized by the bulk fluid speed in the coating-free case while the charge density has been normalized by its maximum value. The radial distance is in units of the inner radius of the tube. The fluid density is $0.8\sigma^{-3}$ while the bulk and surface charge densities are $0.02\sigma^{-3}$ and $0.1\sigma^{-2}$, respectively. The coating has a grafting density of $0.05\sigma^{-2}$ and degree of polymerization $N = 20$. Further details can be found in [128, 124]. The schematic representation of the system is roughly aligned with the graph.

exponential decay as predicted by Debye–Hückel theory. The slight bump in this curve is the result of packing of the water beads near a fixed corrugated wall. This effect is even more evident if one looks at the individual ion density profiles. The fluid velocity (dotted curve) changes in the region where there is a net charge but takes on a bulk value outside of the thin charged region near the wall.

For microfluidic devices with complex geometries the EOF profile is often non-trivial to find. For the entropic trapping device developed by Han and Craighead [125], simulations were carried out using DPD with a slip boundary condition to reproduce a realistic EOF profile in order to include its effects in more complex simulations [126]. Similarly, it has been shown that the LB method can also be used to effectively model EOF [127]. The problem of EOF in complex geometries has also been investigated by solving the Navier–Stokes equation numerically [6]. In fact, the only fluid model presented in this review that has not been used for modeling EOF to our knowledge is the recently developed SRD algorithm.

In the context of electrophoretic separation, the presence of EOF often has a deleterious effect on the resolution. For example, the EOF increases dispersion in capillary electrophoresis because the EOF is non-uniform due to the non-uniform charge distribution on the wall [5, 124, 129]. For this reason, polymer coatings are often used to quench the EOF. They have the additional benefit of preventing wall–analyte interactions that cause additional dispersion in the system [130]. Simulations of polymer coatings tend to use a system size that is thicker than both the Debye layer and the polymer coating. Beyond the counterions and polymer coating the fluid velocity profile reaches a plateau. The fluid speed in this plateau region (referred to as the bulk speed) is the same regardless of the system size and thus these miniature (often nano-scale) simulation systems provide realistic models for much larger experimentally relevant systems.

Simulations of EOF in the presence of a polymer coating are fairly recent due to the high computational overhead involved in simulating them. Recent numerical investigations [124, 128] have been able to reproduce the scaling predictions of Harden *et al.* [131] for grafted polymer coatings using coarse-grained MD simulations. These studies looked in particular at the case when the polymer coating is thicker than the Debye length and looked at two regimes: the mushroom (isolated chains) and brush (high grafting density). In both regimes the MD simulations were able to confirm some of the predicted scaling behaviours of the bulk EOF with respect to the properties of the polymer layer such as the scaling with respect to the degree of polymerization N and grafting density. The dashed line in Fig. 4 shows a simulation where a polymer coating of length $N = 20$ beads and grafting density of $0.05\sigma^{-2}$ is used (here σ is the bead size in the WCA potential, Eq. (4)). Even these relatively short polymers clearly quench the majority of the EOF in the bulk of the fluid (note that in experiments the thin region near the wall where flow is generated makes up

only a very small fraction of the total system size). Simulations by Qiao and He [132] using the DPD algorithm investigated the same situation showing interesting non-linearities in the EOF due to dynamic coupling between the polymer's conformation and the fluid velocity profile. The simulations also confirmed the fluid velocity profile as a function of the distance from the wall for a quenched polymer brush.

More detailed atomistic simulations by Qiao [133] have shown that for cases where the Debye layer is on the same scale as the polymer layer more complex behaviour can result. They found that at low grafting densities hydrophilic polymer coatings can actually increase the thickness of the Debye layer and thus the potential difference between the wall and the bulk fluid (termed the zeta potential) which increases the bulk EOF. This effect was attributed to a reduction in the amount of water in the region of the polymer layer, which caused the counterions to move further from the surface. At higher grafting densities, a larger suppression of EOF as the friction between the polymers and the fluid becomes larger was shown.

3.2 Free-flow electrophoresis

Free-flow electrophoresis is widely used to separate and characterize biomolecules. When a polyelectrolyte in gel-free solution is subject to a constant electric field, its average drift velocity depends not only on the applied field but also on interactions between the polyelectrolyte, the counterions and the solvent. Because the interrelation between the different forces is quite complex, free-solution electrophoresis is not easily accessible to complete analytical treatments. Results do exist for long-chain limits where certain simplifications are applicable [134–136] but experimental evidence indicates that these models are not sufficient to explain the behaviour of short chains [137–139].

In the schematic of the free-solution electrophoresis of flexible polyelectrolytes (Fig. 5), we see that the mobility is a function of length that approaches a constant with increased chain length so that separation of longer macromolecules by electrophoresis is not possible. This limit, called the free draining regime, is well described by analytical methods [134–136].

The behaviour of short chains, exhibiting not only length dependence but a non-monotonic behaviour in the transition from oligomers to long flexible chains, is not adequately described by current theoretical approaches. Here, modern simulation methods introduced in Section 2 provide much insight. The ability to coarse-grain certain interactions more than others facilitates probing different aspects of the behaviour one at a time.

In particular, fully atomistic MD (Section 2.1) can look at small oligomers, thereby focusing on chemical details, and has been employed to accurately describe the dynamic behaviour of short (3 and 6 units) fragments of ssRNA [140]. The diffusion coefficient (corrected for finite-size effects
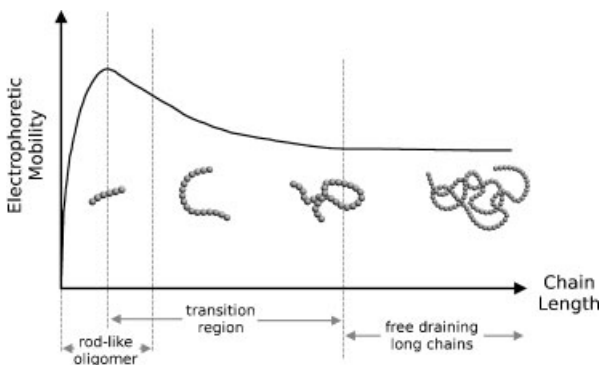
Figure 5. Schematic of the dependence of the electrophoretic mobility on the length of a flexible polyelectrolyte in free solution. Short rod-like oligomers show a sublinear increase in electrophoretic mobility with chain length. The mobility approaches a constant for long globular chains in the free draining regime. Between these two behaviours lies a transition region in which both counterion and hydrodynamic effects must be accounted for.

[141] and solvent viscosity) and the increase in electrophoretic mobility from 3 to 6 nucleotides are consistent with experimental results. The simulations show the importance of the counterions in reducing the effective charge by transiently binding to the polyelectrolyte resulting in the sublinear increase in the mobility with chain length that we see in Fig. 5. The fact that the mobility follows the increase in effective charge demonstrates how the hydrodynamic friction of short, rod-like polyelectrolytes depends only weakly on the length of the chain.

Longer-chain behaviour can be understood only by investigating the hydrodynamics of polyelectrolytes undergoing conformational changes from a rod-like to a globular state. As the number of counterions bound to the polyelectrolyte increases with length, in this midlength regime their contribution remains essential. Two recent studies using mesoscopic techniques (SRD (Section 2.3.2) and LB (Section 2.3.3)) have investigated the transition region between short fragments and long chains in detail [142, 143]. They show that without HI, mobility would actually decrease with length and approach a constant value for large molecular weights. However, by including HI, simulations accurately reproduce the experimentally observed non-monotonic behaviour of the mobility. By determining the effective charge, estimates of the effective friction were determined, and a transition from logarithmic to linear scaling with length was observed [144]. The microscopic interpretation of this phenomenon is still being discussed, but all of these studies [142–144] emphasized the importance of the interplay between HI and counterion condensation. This change is attributed to the correlated movement of the counterions in the vicinity of the polyelectrolyte, effectively cancelling long-range HI this signals the transition to a free draining regime.

When the chain length is increased further, screening eliminates the need to explicitly account for hydrodynamic

effects. In this case, implicit fluid techniques without hydrodynamics (Section 2.4) but with explicitly included counterions have been applied to study polyelectrolytes in electric fields, showing that below a critical field strength the static and dynamic properties of the polyelectrolyte remain unaffected and continue to agree with experimental data. However, when using high electric field strengths that exceed the fields in experiments by several orders of magnitude, alignment of the polyelectrolyte with the field and an increased electrophoretic mobility due to dissociation of counterions is observed [145, 146]. Whether these effects are of any practical relevance is not clear.

The above works emphasize the importance of correlations between counterions, the polyelectrolyte and the resulting screening of HI. Unlike the electrophoretic motion, the diffusive motion of the polyelectrolyte is not correlated with counterion motion and HI remain unscreened [143, 147]. It has been shown that the diffusion of long polyelectrolytes can be correctly modelled when the counterions are neglected as long as hydrodynamic effects are included [148]. In this simulation, the Rotne–Prager–Yamakawa formulation (Section 2.4.2) was used to quantitatively predict equilibrium and non-equilibrium diffusivity of DNA molecules up to 126 μm in length.

3.3 Polymer-obstacle collisions

In many electrophoretic methods, size selectivity is due to the interaction between the analyte and obstacles of some sort. To better understand this interaction, Deutsch and Madden [149, 150] have done pioneering 2-D BD simulations of a polymer migrating through an ordered matrix of obstacles. These authors found that in a very strong field, the polymer migrated through the gel in an unexpected fashion, very different from the conventional reptation picture [103]. The chain goes periodically through a sequence of states: a coil collides with a post, extends its arms around it, slides off the post leaving it in a fully extended state, and then collapses into a coil again. This process, termed geometration, was later observed in videomicroscopy experiments [151, 152]. Collision with a post is an important part of geometration; obviously, this process can be studied computationally in more detail if a system with just a single obstacle is considered.

Nixon and Slater [153] did the first such computational study using the BD approach in 2-D. They considered a chain of beads (without excluded volume) connected by FENE-like springs inside a narrow channel with an obstacle. The field was assumed to be uniform, *i.e.* the field lines penetrate the obstacle. The chain started in the random coil state. As the collision begins, the coil gets deformed and becomes pancake-shaped. The subsequent behaviour of the polymer is similar to that observed by Deutsch and Madden, but more clearly seen, as other neighbouring obstacles do not interfere. Based on these simulations, the authors developed an analytical theory predicting both the average

retardation of the polymer due to the collision and the variance of this retardation.

More detailed simulation studies of collisions using a very similar 2-D BD approach were carried out by Sevick and Williams [154] and Saville and Sevick [155]. The latter studied the properties of collisions as a function of the impact parameter, the initial distance in the direction perpendicular to the field between the centre of mass of the chain and the centre of the obstacle. Different obstacle sizes were also considered. These authors found that besides the "hooking" collisions studied by Nixon and Slater, another possibility is the "rolling off" collisions where the coil "rolls over" the surface of the obstacle and does not deform much during the collision (Fig. 6). For "rolling off" collisions that become dominant for large obstacles, the duration of the collision depends mostly on the obstacle size, rather than the chain length. Among "hooking" collisions, besides the conventional type (called U/J collisions, because the hooked chain conformation resembles these letters), collisions with multiple hooking (later termed W collisions [156], as the conformation can resemble a "double-U") were also found.

More recently, Randall and Doyle [157] found in their fluorescence microscopy experiments that besides U/J and W collisions, yet another type of collision (called X for "extending") is possible. These collisions resemble the U/J type, but the longer arm of the chain is not fully unwound at the beginning of the unhooking process, containing a coil at the end that unwinds gradually as the unhooking proceeds. To study this collision type in detail, Kim and Doyle [158] carried out 3-D BD simulations with excluded volume interactions. Unlike previous work, they did not make the assumption of a uniform electric field, instead calculating the field assuming that the obstacle (cylindrical in shape) is a perfect insulator. They indeed found X collisions, along
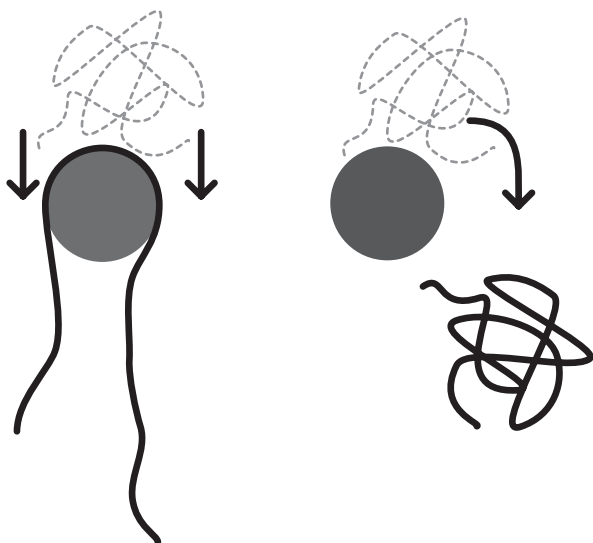
Figure 6. Different types of collisions of a chain with an obstacle: a collision involving hooking of the chain upon the obstacle (left) and a "rolling off" collision during which the chain remains a coil (right).

with previously known U/J and W types. It turned out that, surprisingly, the X type is the most dominant one in a broad range of chain lengths and field strengths. Given that this remains the case even in simpler models, perhaps previous authors simply did not distinguish between completely and incompletely unwound chains (for instance, [153] did not distinguish between these states).

The work discussed so far deals with the case of strong fields, when the thermal effects are negligible or at least secondary. A very recent paper by Holleran and Larson [159] also considers the case when, on the contrary, the field is weak and thermal diffusion dominates. In this case the arms are never extended and the polymer remains a coil that drifts slowly past the obstacle. In fact, in this regime the polymer, at least semi-quantitatively, can be considered as a rigid particle and be studied using, *e.g.* the exact MC methods described in Section 2.6.1. The paper is also interesting because of its use of a novel computational model of the chain (developed by the authors and described in a separate publication [160]), where the springs connecting the beads and not the beads themselves are repelled by the obstacles, which ensures that the chain cannot penetrate the obstacle even when the distance between the beads is much larger than the obstacle size. This allows the authors to treat very long chains (longer than 1000 Kuhn lengths).

All simulations discussed so far used BD neglecting Coulomb interactions between monomers and HI. Coulomb interactions are screened by counterions. The justification for neglecting HI offered by Kim and Doyle [158] is that both their simulation and the experiment it models [157] were carried out in a slit, in which case HI should be screened. However, even in the bulk the results are at least qualitatively correct, as the comparison with recent simulations by Kenward and Slater [161] using *explicit solvent* shows. Introducing a solvent can certainly produce some quantitative changes. Neglecting HI assumes that the polymer is free-draining, which is true in free solvent, but not when the chain is slowed down by an obstacle. The result is the modification of the friction force on the chain, which also becomes conformation-dependent. Kenward and Slater also studied collisions between two polymer chains, of which only one is driven by an external force, but both are mobile. Such collisions are important in the case of electrophoresis in polymer solutions [162, 163]. In this case, hydrodynamic effects influence the conformations of the chains. Similarly, studying situations where the colliding chain is driven by a flow, rather than an external field, is, of course, possible only when the solvent is included in some way; Kenward and Slater considered this case as well.

Finally, we mention other computational approaches applied to this problem. Starkweather *et al.* did off-lattice bead–rod MC simulations of a chain colliding with an immobile random coil [164] and a mobile chain [165]. As mentioned MC methods often have problems in strong fields, and their use is especially dangerous when applied to this problem, as it involves U-shaped chain configurations. The authors had to restrict themselves to moderate field

strengths, when the chain is far from being fully stretched. André *et al.* [156] used a special algorithm tracking the evolution of different loops and arms of the chain after the impact.

3.4 Ogston: Modeling sieving in hydrogels

A specific electrophoretic regime exists when the size of the analyte is smaller than or comparable to the mean pore size of the gel. This regime is often called the Ogston regime for electrophoretic sieving. Although the concept is technically restricted to rigid analytes, it is possible to extend its use to flexible polyelectrolytes such as DNA if one assumes that the chain takes on a spherical conformation with an effective radius R. By coarse-graining out the fine details of the individual monomers and considering the analyte as a solid sphere, we can discretize our system on a lattice (Fig. 7) and use simulations or exact calculation methods to study the electrophoretic mobility or diffusion coefficient of the analyte in this regime. A straightforward lattice approach to modeling the gel system would be to consider a gel fibre as an impenetrable obstacle. In Fig. 7, the analyte and the obstacles are of the same size (the lattice step size); although this is the case that we will consider below, it is equally easy to study larger obstacles and/or larger analytes that occupy more than one lattice unit (more on this later).

The first such numerical model was used by Slater and Guo [166] to test the key hypothesis of the Ogston–Morris–Rodbard–Chrambach (OMRC) model. According to the OMRC model, the mobility of the analyte in this regime is linearly proportional to the fractional gel volume that it can occupy, a purely geometric parameter that can be computed quite easily for the model shown in Fig. 7. All the other assumptions of the OMRC model (*e.g.* a low field intensity) being compatible with the numerical model, the results of the study represented a direct test of the fractional volume hypothesis. The Slater and Guo exact numerical calculations showed that the mobility of the analyte is higher in an ordered gel, compared with a random one, even if the fractional volume is the same. This was the first demonstration that the OMRC model is incomplete; in fact, these
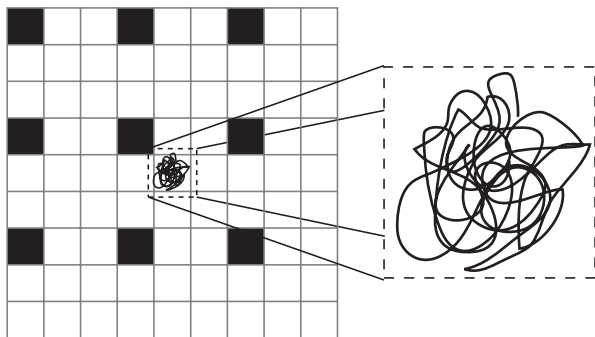
authors also showed that the OMRC model corresponds to a mean-field model valid for an annealed gel (a gel with rapidly moving obstacles) [166].

As mentioned earlier, it is possible to extend the exact method to treat larger particles [167]. In this case, molecules are also viewed as rigid spherical particles, but can be larger than the obstacles. These results are valid in the zero-field limit since the interactions with the obstacles are assumed to be hard-core, *i.e.* the particles do not deform when colliding with an obstacle. It is also possible to extend this calculation method to treat attractive interactions between the analyte and the gel structure [168].

DNA molecules can also be modelled using the MC exact calculation method without making the hard sphere approximation [121]. Indeed, one can use multiple particles linked by bonds to represent a flexible chain. For example, such polymers can be described by self-avoiding walks and modelled by the BFA. This extension opens the door to a fundamental study of the electrophoretic sieving of oligomers, rod-like molecules, vesicles, star-shaped macromolecules, *etc.* One could argue that the MC exact calculation model is not a sufficiently good representation of a gel matrix since the field is assumed to be uniform throughout the gel. In reality, the field lines are affected by the gel structure (the obstacles). It has been shown [169] that the LMC exact method can also be extended to treat spatial variations of the electric field, and that this has little impact on the results at low field intensity.

It is possible to apply the exact method to treat high fields instead of vanishingly small external fields [105]. For non-deformable analytes, this can reproduce the trapping that sometimes occurs in real electrophoresis experiments. Multiple obstacle geometries have been studied and it is possible to properly model experimental observations of trapping and pulsed field de-trapping. A modified version of the initial algorithm [170] also allows the simultaneous calculation of the mobility and of the dispersion coefficient; this is obviously needed in order to predict the resolution of a specific device.

3.5 Microfluidic ratchets

The Brownian motion of particles is what gives rise to diffusion. It is possible to exploit these natural thermodynamic fluctuations for the separation of particles by adding an external force that biases the dynamics. Brownian ratchets are devices that use an asymmetry, either temporal or spatial, to drive the motion of a Brownian particle even when the net external force is zero. For example, a temporal asymmetry could be a zero-mean field alternating between a short high-intensity forward pulse and a longer low-intensity backward pulse. A spatial asymmetry could take the form of asymmetrically shaped obstacles or walls. Using any or all of these types of asymmetry, a non-zero net velocity can be observed in the presence of a field even if the net force is zero (hence the name *ratchet*). The random motion of the

Figure 7. Modeling a polyelectrolyte in the Ogston regime with an LMC model.

particle then plays a major role (this is why it is called a *Brownian ratchet*).

As an example, consider the case of particles in a properly designed microfabricated array of obstacles (see Fig. 8). LMC methods can be used to simulate Brownian ratchets of this kind (see Section 2.6.1.1). First, the system is represented as an array of impenetrable obstacles. A starting point is chosen and the particle is moved randomly with the probabilities defined in Eq. (16). With this method, long computational times would be required in order to obtain statistically precise results. A faster and more precise computational method was described in Section 2.6.1.1 The increased accuracy is vital at very low fields, where the statistical uncertainty associated with the normal approach is often larger than the studied behaviour.

Gauthier and Slater [171] examined several ratchet systems using this simulation approach. The system shown on the right-hand side of Fig. 8 is interesting since it uses a symmetric array of obstacles together with an asymmetric pulsed field. These authors observed several current reversals (changes in direction) for different values of the field. For certain choices of parameters, particles of different sizes but having the same charge were predicted to move in opposite directions, a remarkable result (in some cases, a particle can even move against the direction of the net field, a phenomenon called absolute negative mobility). A Brownian ratchet of this type was later built experimentally by another group [172]. An aqueous solution of charged spheres of radius 2 μm was placed in a periodic array of misaligned posts with alternating small and large gaps. The applied asymmetric external field was a superposition of a constant (E_{DC}) and an alternating signal ($\pm E_{AC}$). The system behaved as expected and absolute negative mobility was observed – a nice example of the kind of new ideas that simulations can suggest.
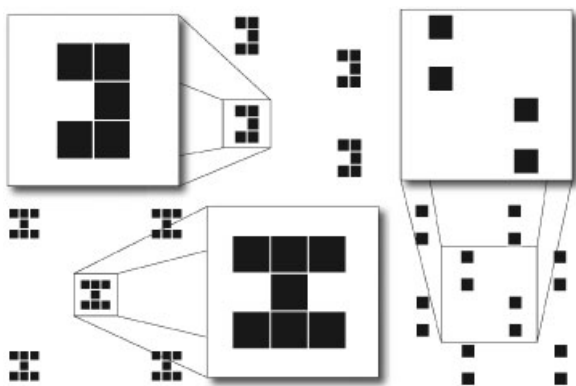
Figure 8. Three types of obstacles that can be used to design a Brownian ratchet separation system. Left, top: trap-shaped obstacles with a left-right spatial asymmetry. An unbiased AC electric field would lead to a net velocity pointing in the negative *x* direction. Left, bottom: symmetric obstacles with traps in both directions. Here, one would need an asymmetric pulsed field to drive the Brownian ratchet. Right: the distribution of obstacles proposed by Gauthier and Slater [171]: misaligned rows of obstacles. The lattices are not explicitly shown for clarity purpose.

Tessier *et al.* [173, 174] studied the system proposed by Han *et al.* [175] in the ratchet regime, both spatial and temporal. For the spatial asymmetry, the system was modified to introduce a geometrical asymmetry. The BFA (see Section 2.6) was used to model the polymer. Tessier *et al.* also simulated the system using a zero integrated pulsed field [176]. In both cases, separation was predicted. These predictions have yet to be tested.

3.6 Nanopore translocation

By threading ssDNA through a narrow pore (Fig. 9) and identifying the bases as they pass through, nanopores offer a promising avenue for the development of sequencing technologies [177]. In contrast to gel electrophoresis, nanopore sequencing could offer rapid (thousands of bases *per* second) sequencing of a single DNA molecule; a revolution which would have a great impact in fields associated with the life sciences. The same approach can also be used for other purposes, such as sizing molecular contour lengths. A significant advancement occurred in 1996 when Kasianowicz *et al.* demonstrated that RNA and DNA could be detected passing through a biological nanopore (α-haemolysin) by monitoring the disruption of ionic currents [178]. Subsequently, there have been a great number of theoretical [179–182] and experimental studies [183–188] focused on nanopore translocation (note that the number of nanopore related publications is staggering and in this very brief review, we are limited to providing only a few selected publications for each topic). Providing a bridge between theory and experiment, many computer simulations have also been performed and, in fact, most of the techniques discussed in Section 2 have been used to study the translocation process.

At the coarsest level, LMC simulations (see Section 2.6.2) are often performed in conjunction with theoretical studies to test the resulting predictions [181, 182, 189–193]. Other studies have used off-lattice MC to study translocation driven by an external or adsorption force [194–196]. Finally, one approach has mapped the translocation onto a 1-D diffusion process and then employed an exact numerical technique to obtain results [122, 197]. Although such studies are able to investigate very long polymers at low fields, the details of the dynamics are not produced and, additionally, the model is coarse to the extent that effects such as HI can be included only in an approximate manner. At the opposite end of the spectrum, fully atomistic MD simulations of DNA inside a channel have also been performed. These studies have revealed interesting details about the viability of distinguishing between bases of DNA translocating through a synthetic nanopore [1] and the dependence of various quantities on the DNA orientation inside the biological α-haemolysin channel [198]. They are, however, limited in terms of time scale and are unable to simulate the full translocation process. In between these extremes, many coarse-grained MD simulations using an implicit fluid [199–201], an explicit fluid
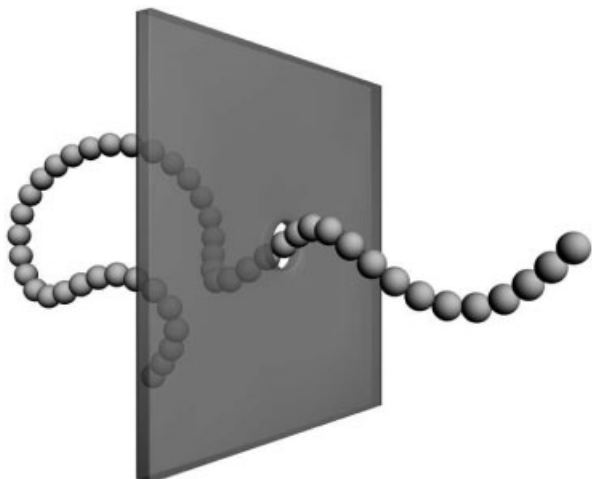
Figure 9. Schematic of a polymer translocating through a solid-state nanopore.

[202–204], or a mesoscopic fluid model [205–208] have been performed in an attempt to include the critical factors while requiring a reasonable level of computational power.

Using one or more these approaches, these studies have investigated the role of underlying physical mechanisms such as conformational entropy [197], HI [205], the solvent effect [209], counterions [204], pore-polymer interactions [210], and the pore geometry [211, 203]. Additionally, the dependence on the nature of the polymer has been studied by simulating charged polymers [212] and heteropolymers [213, 214]. Furthermore, considering application to sequencing, it is not surprising that a great number of studies have also examined driven translocation by implementing a pulling force [215], an adsorption force [196], or an external field (discussed below). As is obvious from this list, which is in itself incomplete, there is not enough space in this brief review to cover all of these results. Rather, as a single example, we will discuss some of the results for a key aspect of the general translocation problem: the scaling of the translocation time τ with the degree of polymerization N of the polymer for driven translocation.

In experiments on the biological α-haemolysin pore, both Kasianowicz *et al.* and Meller *et al.* found a linear dependence of the translocation time on the polymer length ($\tau \sim N$) for short ssDNA fragments [178, 188]. In contrast, the experiments of Storm *et al.* found a scaling of $\tau \sim N^{1.27}$ when driving long DNA strands (6500–97000 base pairs) through a solid-state nanopore [183]. This result is in agreement with their prediction that $\tau \sim N^{2\nu}$ for long polymers when HI are taken into account ($\nu \cong 3/5$ is the 3-D Flory exponent). From the analytical side, considering translocation driven by a chemical potential gradient, Muthukumar predicted linear scaling [189] while Kantor and Kardar predicted $\tau \sim N^{1+\nu}$ [191]. The latter group also performed bond-fluctuation MC simulations but were unable to verify the prediction due to limited polymer lengths. However, additional simulation studies for long

polymers have found a scaling of $\tau \sim N^{1+\nu}$ using 2-D fluctuating bond MC [216] and using the exact numerical method [197]. Finally, Dubbeldam *et al.* predicted a scaling of $\tau \sim N^{2/(2\nu+2-\gamma_1)}$ (where γ_1 is the surface exponent) [217] and found results consistent with this from off-lattice MC simulations. Moving towards a more detailed simulation of the dynamics, driven translocation has also been studied using LD and BD simulations. Performing 2-D LD simulations, one study found a scaling of $\tau \sim N^{1+\nu}$ [201] – a result consistent with the Kantor and Kardar prediction and the MC simulations cited above. Meanwhile, others have found a linear dependence [199, 200]. The discrepancies between these results may be attributed to differences in the particular system setups such as the pore length, polymer length, magnitude of the external field, and polymer model.

A limitation of all the simulation results cited thus far (MC and LD/BD) is that they neglect HI. As long ranged correlations through the fluid are conceivably important in the translocation process, much of the current work focuses on MD simulations using mesoscopic fluid models. Using the DPD approach, He *et al.* have found a linear dependence of τ on N [207]. Meanwhile, Izmitli *et al.* [205] and Fyta *et al.* [206], each using an LB fluid model but with different polymer models, have both found an exponent of 1.28, a result in good agreement with the experimental data of Storm *et al.* corresponding to $\tau \sim N^{2\nu}$. Both of these studies also directly tested the impact of HI by performing the same simulations without the LB solvent. Izmitli *et al.* found a negligible change as the exponent rose to 1.31 while Fyta *et al.* observed a slightly larger effect with the exponent rising to 1.36. The key parameter here appears to be the molecular size: is there a critical polymer size below which the HI are negligible because the translocation is then dominated by the polymer-pore interaction and not by the polymer-fluid interaction? In our opinion, a combination of careful simulations and experimental studies will be needed to answer this question.

As demonstrated by this one example, a wide range of simulation techniques have been employed to elucidate various details of the translocation process. In fact, given this wide array, one must keep in mind the scope of a particular simulation approach and the limitations of a chosen system setup when considering the results of each study. Ultimately, however, this diverse amount of information is an advantage in fully characterizing the system. While there are still many hurdles remaining before a nanopore sequencing device is realized (the development of a base identifying detector, slowing down the overall process, having the DNA find the pore), current simulations are giving insight on the fundamentals of polymer translocation.

3.7 Entropic trapping

In Ogston-type models of electrophoresis, it is assumed that analytes cannot pass through constrictions that are smaller

than their diameter. This is true for hard particles, but polymer coils can deform and still pass through holes that are much smaller than their radius of gyration R_g. However, as deformed coils are no longer completely random, this has an entropy cost and a polymer entering a narrow space has to overcome an *entropic barrier*. In a porous medium, such as a gel, such barriers are especially important when the average pore size is comparable to R_g so that there are pores both smaller and larger than R_g. In this situation, *entropic trapping* is possible, in which case the polymer can stay trapped for a long time in a large pore, since all ways out of it involve overcoming entropic barriers. The consequences of this were first studied in off-lattice MC simulations (Section 2.6.2) by Baumgärtner and Muthukumar [218–220]; one interesting result is a much stronger size dependence of the diffusion coefficient (and thus, *via* the Nernst–Einstein relation (Section 2.6.1), of the electrophoretic mobility) than predicted for larger polymers spanning many pores (the reptation regime). This was later confirmed experimentally [221].

Entropic trapping in gels, while an important issue, is still just one of the factors influencing the separation. On the other hand, Han *et al.* [124, 175, 222, 223] have fabricated and studied a device where, by design, entropic trapping is the dominant contribution to separation. The device is an array of cavities separated by long and narrow *slits*. The size of the cavities is much larger than R_g for the typical DNA sizes whose separation is desired, whereas the width of the slit is much smaller than R_g in one direction, but, importantly, is still $\gg R_g$ in the other direction. Han *et al.* found that the mobility *increases* as the size of the polymer increases. This is rather counterintuitive, given that larger polymers should deform more passing through the slit and this should be more entropically costly. Han *et al.* explained this by suggesting that rather than entering the slit as a whole, the polymer stays around the slit and loops (or *hernias*) get inserted in the slit (Fig. 10). Such insertion has an entropy cost proportional to the insertion length, but it also causes the decrease of the electrostatic energy proportional to the square of the length. As a result, the free energy increases until the top of the free energy barrier is reached, but then starts decreasing. The escape rate, as always in transition-state theory, depends exponentially on the barrier height, but also depends on the prefactor (the attempt frequency). It was argued that the barrier height is inversely
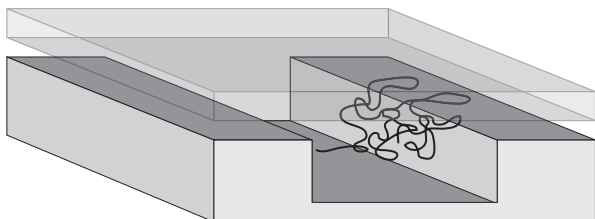
proportional to the field strength, but is independent of the polymer size, and so the separation is entirely determined by the prefactor. This prefactor should be proportional to the size of the part of the polymer exposed to the slit, as this determines the number of hernias that can form simultaneously; this size is proportional to R_g which increases with the polymer size, and therefore the escape rate indeed increases with the size, as observed experimentally.

This simple theory, while appealing, was in need of verification by simulations, especially given that it relied on the independence of the free energy barrier height of the polymer size; since this barrier height enters in the exponent, even a slight dependence may completely overwhelm the dependence contained in the prefactor. With this in mind, several simulations have been carried out. Tessier *et al.* [173] used the MC BFA (Section 2.6.2.3). The field used in the simulation was computed by numerically solving the Laplace equation. The results for the mobility obtained in the simulations are in qualitative agreement with the experiments. Overall, the simulations confirmed the theory by Han *et al.*, but also further refined it. In particular, it was found that for weaker fields the mean trapping time indeed depends exponentially on the inverse field with the slope on the semilogarithmic plot independent of the molecular size, confirming that the activation energy is indeed size-independent. On the other hand, for longer chains there was a deviation from the perfect exponential at higher fields attributed to the change in the shape of the coil near the entrance to the slit. At moderate fields the coil around the slit acquires a pancake shape and the radius of gyration behaves as that of a *2-D* random walk; but as the field gets stronger, the escape into the slit is so fast that the coil has no time to deform. This has obvious consequences for the escape rate, as the prefactor depends on the extent of the coil along the slit entrance. The field dependence of the critical hernia length, as estimated by Tessier *et al.*, is also largely in agreement with the theory.

Chen and Escobedo [224] looked more directly at the free energy barrier associated with the entrance into the slit. Since free energy calculations are done in equilibrium, one of the equilibrium MC methods (in their case, configuration-bias MC [225]) was used (see Section 2.6). The advantage of this approach is that reliable results can be obtained even for very small fields, when the escape is so slow that good statistics cannot be obtained in dynamical simulations. The result of these free energy calculations is that over a large range of parameters, the barrier height is indeed polymer-size-independent, however, deviations are observed at very low fields for very short chains (the regime that Tessier *et al.* could not study very carefully). These deviations are not unexpected: at very low fields, the critical hernia length is very large, and if the chain is short, may actually become comparable to or even (in theory) exceed the chain length.

Streek *et al.* [226] used BD simulations (Section 2.4) to study essentially the same system. Based on their results, these authors suggest that in addition to entropic trapping, there exists another separation mechanism, due to size-dependent trapping of chains in the corners of the

Figure 10. Schematic drawing of a part of the entropic trap device of Han *et al.* with a DNA chain near the entrance to a narrow slit. Several hernias are inserted in the slit.

cavity. The authors claim that it is this new mechanism, rather than entropic trapping, that is dominant. This may well be true at the rather high fields that they consider and especially in the case of constrictions that are wider than the radius of gyration of the chain (considered in a separate publication [227]), when the entropic barriers are essentially negligible. On the other hand, it is clear that at very low fields for narrow constrictions the entropic trapping mechanism should dominate, as no mechanism based on diffusion alone, without any activation barriers involved, would be able to compete. The intermediate case, when the entropic barrier height is $\sim k_B T$, is the most interesting practically and deserves further study; the answer may depend on many details, such as the size of the cavities.

We should also mention newer work likewise using BD. Panwar and Kumar [228] recognized that when the trapping barrier is not very high, two other time scales besides the trapping time contribute: the time it takes the DNA to approach the constriction and the crossing time. They studied the field and chain length dependencies of all three times. These authors used a bead-rod model of the DNA; Lee and Joo [229] did a similar study for a bead–spring chain.

All work described here uses methods that do not take hydrodynamic effects into account. For this reason, the DNA behaves as a free-draining chain when in reality a trapped chain is not free-draining. As Tessier *et al.* [173] point out, this implies that the field intensity needed to overcome the entropic barrier is underestimated by a factor of $\sim N^{2/5}$, where N is the chain length. As always at this level of modeling, quantitative comparisons with experiment are difficult, because the effective charge of the DNA is different from the bare charge due to counterion condensation. These effects need to be taken into account in future work.

### 3.8 Surface electrophoresis

A novel electrophoretic separation technique based on the DNA's interaction with a surface was first reported by Pernodet *et al.* [230] in 2000. By adsorbing DNA to a surface, length dependent separation on a flat surface without any restrictions or any sieving matrices was achieved (see Fig. 11A). It was found that the interactions between the molecule and the substrate essentially act as a length dependent source of friction, enabling electrophoretic separation. The initial experimental observations were accompanied by MD simulations [231, 232] and have been followed up by further studies [233, 234] under different conditions. The results showed that the DNA-surface interaction is a key parameter for the process: a strong attraction leaves the molecules fully adsorbed and no separation is possible, too weak an attraction lets molecules desorb and resume bulk behaviour, where likewise no separation is possible. Additionally, the interaction can be noticeably influenced by choosing a specially patterned surface [235, 236], an exciting and unique approach to designing optimized and custom-made separation systems.

Since the exact nature of the interaction and the resulting separation mechanism remain elusive at this point, there is a pressing need for more elaborate theoretical and computational studies that include electrostatic and hydrodynamic effects alike as they are crucial when the molecules approach the surface. This has been neglected so far.

3.9 Confinement-driven separation

Recent progress in design and fabrication of microfluidic devices on a sub-micrometer length-scale [237–239] demands a good understanding of the statics and dynamics of the polyelectrolytes under steric confinement. We can distinguish several regimes of confinement. In a device that is much larger than the size of the polyelectrolytes, given by their radius of gyration R_g, the conformations are unperturbed and isotropic (weak confinement). Reducing the dimensions of the devices to the order of R_g, the conformations of the polyelectrolytes start to become restricted by the walls and show deviations from the equilibrium (strong confinement, see Fig. 11B). With further reduction of the device size, the polyelectrolyte becomes extremely restricted and the static and dynamic properties undergo significant changes [240, 241] (Fig. 11C).

The decrease in size of microfluidic devices used in actual experiments and the growth in size of the systems that are addressable by means of computer simulations – due to advancement of simulation methods together with the increase of computer power – led to a cross-over creating systems that can be worked on from both sides. Recent experiments in slit-like nanochannels studied the static and dynamic properties of single molecules [242–248] and showed how confinement can be used as a tool to change polymer conformations as well as the dynamics through
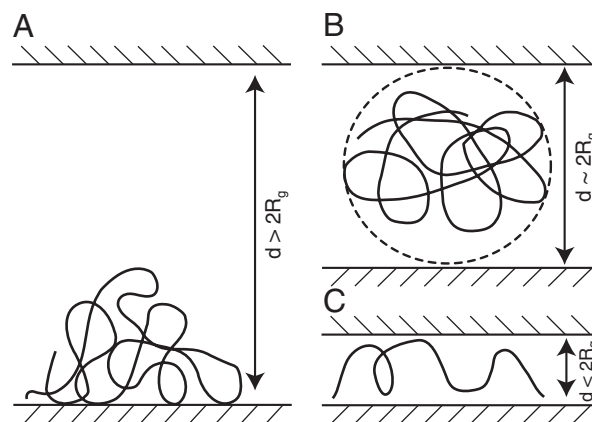
Figure 11. Different regimes of confinement used in some gel-free separation techniques: (A) weak confinement ($d > 2R_g$) in the presence of an attractive surface, (B) stronger confinement ($d \sim 2R_g$) that starts to influence the chain conformations, and (C) strong confinement ($d < 2R_g$) in which the chain conformations are determined by the walls of the channels.

modulation of the HI. Consequently, the role of hydrodynamics in confinement has been the focus of several recent computer studies [75, 96, 248–254]. The results indicate that, under weak confinement, the HI between polymer and wall drive the polymer to the centre of the channel if an external flow is applied. However, in high confinement, a migration towards the channel walls was observed. Since this interesting physical phenomenon depends on the ratio of the size of the polymer to the width of the channel as well as on the strength of the driving force, it seems to be an ideal candidate for free-solution separation of polyelectrolytes. Recently reported measurements on the diffusion and the electrophoretic mobility of DNA in strongly confined systems [255–257] indicate a possible electrophoretic separation mechanism based on the modified dynamics in strong confinement. A systematic simulation study of this subject has yet to be done in order to verify these results. In particular, electrostatic interactions and the influence of counterions on the HI have been neglected so far, but they should be assumed to be of great importance if the length scales of the system become comparable to the Debye length, below which electrostatic interactions are not fully shielded by the solvent [258, 254].

4 Outlook

This review has hopefully convinced the reader that the computational approach has been useful in understanding a large variety of electrophoretic separation systems and relevant electrokinetic phenomena. Compared with theory, many situations that cannot be studied theoretically without gross simplifications can be treated computationally; in fact, simulations provide valuable clues to theorists as to *exactly what* simplifications and assumptions they are allowed to make. Compared with experiments, simulations have an unmatched ability to look at the microscopic level; but perhaps the most important is the possibility to "switch on and off" different effects (such as HI) at will, something that is not available to experimentalists and yet is extremely helpful in developing a better understanding of the systems and phenomena of interest.

Considering the future of both the simulation methods and their applications to separation phenomena, the most straightforward approach is the "brute-force" one: harnessing the inevitable increases in computational power to conduct more detailed simulations of larger systems for longer times. However, in striving for more realistic simulations in this manner, it is important to recognize just how wide the gulf between experiments and detailed simulations is. To see this, consider atomistic MD simulations that are already being used to study DNA inside a nanopore (Section 3.6). While these simulations are yielding interesting results, significant increases in computational power would greatly enhance what they are able to study. For example, detailed atomistic simulations may be able to aid in the design of a probe to read the bases as they pass through the channel. However, current atomistic MD simulations are typically limited to trajectories of hundreds of nanoseconds for limited system sizes. On the other hand, in the lab, the dynamics of interest can evolve on a time scale up to seconds or even longer. Consequently, while any increase in computational power is enthusiastically welcomed, the gap between detailed simulation and experiment remains large and the development of efficient techniques to appropriately coarse-grain the simulations is equally vital to broadening the scope and relevancy of computational studies.

Hence, as a final thought to this review, we examine a number of emerging or long-standing-but-difficult areas where new ideas and computer simulations will be needed over the next few years.

4.1 Multiscale simulations

In simulations, often different regions of the system require different levels of detail. For instance, a molecular-level fluid model may be required in the vicinity of the analyte, but at larger distances a faster mesoscopic approach may be sufficient. Likewise, the accuracy of a translocation simulation may be improved if the polymer is simulated atomistically in the vicinity of the nanopore. To avoid simulating the whole system with the highest level of detail needed only in a small region, multiscale simulations can be used. The biggest challenge is the seamless coupling between regions with different level of detail, which is especially difficult if the region boundaries are required to move. Several multiscale methods for fluids have appeared recently (see [259–264]). Such methods should see increased use in electrophoresis simulations. Besides, more "trivial" *serial* multiscale studies, where the outcome of a more detailed simulation is used to construct a coarse-grained model and *vice versa* [265], will be useful.

4.2 Mesoscopic solvents

SRD is a relatively new method of mesoscopically handling solvents and as such its full potential has yet to be captured. Despite being a model that is conceptually and relatively simple to implement, few of the electrophoretic simulation examples discussed above have taken advantage of SRD's ability to treat relatively large and multicomponent systems with complex and dynamic boundary conditions. Furthermore, careful choice of the multiparticle collision operator allows for hydrodynamics to be "turned off" and simply replaced with a Brownian heat bath in order to explore HI effects in the system.

4.3 Hydrodynamic effects in gel electrophoresis

The separation of small analytes by gel electrophoresis is often called "sieving". "Small" typically means that the size

of the object is smaller than the mean pore size of the gel matrix. The word sieving suggests that separation is related to steric interactions restricting the motion of the analyte. Although detailed obstruction models have been proposed, their validity is not clear because they ignore HI and do not properly treat electrostatic interactions. Since we have three length scales here (the Debye length, the particle's radius and the mean pore size), many different regimes must exist. Understanding the simultaneous screening of the electrostatic and HI in a sieving matrix, especially if the latter is an entangled polymer solution, will require new ideas and probably extensive coarse-grained MD simulations.

4.4 Electrophoresis in polymer solutions

Electrophoresis in capillaries and microchips using polymer solutions as sieving matrices is increasingly important. Conventional wisdom is that well-entangled polymer solutions behave essentially like gels. However, the absence of crosslinking may be important, especially in strong fields typically used for capillary electrophoresis. Recent videomicroscopy experiments [266, 267] seem to suggest that the DNA is able to drag matrix polymers even well above the entanglement concentration. Simulations are needed to help understand this process. The consequences for the basic geometration mechanism of DNA motion can perhaps be understood even in rather simple models similar to that by Deutsch [149], but with ''draggable'' obstacles. Electrophoretic motion in more dilute solutions, around the critical entanglement concentration, is of interest as well.

4.5 Drag-tags for free-solution separation

Attaching suitable molecules to DNA fragments can restore size-dependent mobility regardless of the free-draining property [268–270]. The read length is optimized by choosing large but perfectly monodisperse drag-tags. As it is an experimental challenge to produce such polymer labels, two recently proposed alternatives seem promising: Haynes *et al.* [271] proposed to use branched polymers with well-defined architecture, whereas Grosser *et al.* [272, 273] introduced non-ionic surfactant micelles as drag-tags with very large hydrodynamic friction. Computer simulations can be used to characterize these new labels and provide ideas on how to extend these approaches.

4.6 EOF

As mentioned in Section 3.1, it has been shown that the mesoscopic fluid models such as LB and DPD provide realistic EOF profiles. It has also been shown that they provide realistic HI. One would suspect that given that they do these two things accurately, they will probably also be able to model EOF in the presence of polymer coatings.

If this is the case, mesoscopic models could allow for the simulation of more complex coatings and a wider range of parameters due to the increase in speed of computation.

4.7 DNA denaturation

As a means of sequence dependent separation, denaturing gradient gel electrophoresis exploits a rapid decrease in the mobility of a dsDNA fragment when sections of it denature. It is currently unclear whether the experimentally observed blocking is an actual trapping or a steep reduction in mobility. The bubble dynamics could play an important role in the blocking, thus a static helical-coil configuration may or may not be enough to give the correct picture. Unfortunately, simulating accurate bubble dynamics sets a coarse graining length scale to the length of a single base pair. A MD model that could incorporate the correct ''breathing'' dynamics of a dsDNA [274] in the presence of a gel while being able to treat dsDNA lengths of interest could be an important tool for investigating the blocking phenomenon.

4.8 Separation of large DNA

The idea of a Human Genome Project became realistic when PFGE made it possible to separate DNA molecules as large as a few megabase pairs (Mbp), a necessary step for chromosome mapping and sample preparation. After a few years of rapid progress, PFGE saturated at about 5 Mbp. Of course, the physics of PFGE is expected to be complicated for molecules that are millimeters in contour length! Agarose gels, with their sub-μm pores, are probably not the best material to extend the usefulness of PFGE. Recent ideas, based on new separation concepts, have yet to become commercial products. Computer simulations played a key role in the development of PFGE, and will again be needed in order to optimize the separation of such huge molecules and to design new and faster devices.

4.9 Protein separations

While the electrophoretic separation of nucleic acids, small ions and spherical particles has been modelled extensively, the same cannot be said of protein electrophoresis. Proteins are complex molecules, with non-trivial charge distributions on their surface. They can be separated in their native state or denatured, in free-flow electrophoresis or in gels, under uniform conditions or in the presence of gradients of various kinds. Although some models developed for particles or DNA can possibly be used for proteins as well, this has never been carefully tested. Computer simulations will be required to optimize the separation of proteins, which remains a difficult issue in the laboratory. However, generic simulation methods are not likely to work well since the precise shape and charge distribution that characterize a specific protein must be taken into account.

In conclusion, as computers become more powerful and new algorithms are developed, the future of computational studies of separation phenomena looks even brighter!

The authors have declared no conflict of interest.

5 References

[1] Aksimentiev, A., Heng, J. B., Timp, G., Schulten, K., *Biophys. J.* 2004, *87*, 2086–2097.

[2] Noolandi, J., Rousseau, J., Slater, G. W., Turmel, C., Lalande, M., *Phys. Rev. Lett.* 1987, *58*, 2428–2431.

[3] Slater, G. W., Noolandi, J., *Phys. Rev. Lett.* 1985, *55*, 1579–1582.

[4] Slater, G. W., Rousseau, J., Noolandi, J., *Biopolymers* 1987, *26*, 863–872.

[5] Potoček, B., Gaš, B., Kenndler, E., Štědrý, M., *J. Chromatogr. A* 1995, *709*, 51–62.

[6] Patankar, N. A., Hu, H. H., *Anal. Chem.* 1998, *70*, 1870–1881.

[7] Noolandi, J., Slater, G. W., Lim, H. A., Viovy, J. L., *Science* 1989, *243*, 1456–1458.

[8] Olvera de la Cruz, M., Deutsch, J. M., Edwards, S. F., *Phys. Rev. A* 1986, *33*, 2047–2055.

[9] Duke, T. A. J., *Phys. Rev. Lett.* 1989, *62*, 2877–2880.

[10] Zimm, B. H., *J. Chem. Phys.* 1991, *94*, 2187–2206.

[11] Duke, T. A. J., Viovy, J. L., *J. Chem. Phys.* 1992, *96*, 8552–8563.

[12] Graham, R. S., Larson, R. G., *Macromolecules* 2007, *40*, 366–378.

[13] Español, P., in: Karttunen, M., Vattulainen, I., Lukkarinen, A. (Eds.), Novel Methods in Soft Matter Simulations, Springer, Berlin 2004 pp. 69–115.

[14] Rapaport, D. C., *The Art of Molecular Dynamics Simulation*, Cambridge University Press, Cambridge, New York 1995.

[15] Frenkel, D., Smit, B., *Understanding Molecular Simulation*, Academic Press, Orlando, FL, USA 2001.

[16] Allen, M. P., Tildesley, D. J., *Computer Simulations of Liquids*, Clarendon Press, Oxford, UK 2002.

[17] Haile, J. M., *Molecular Dynamics Simulation: Elementary Methods*, Wiley, New York 1992.

[18] van Gunsteren, W. F., Berendsen, H. J. C., *Angew. Chem. Int. Ed. Engl.* 1990, *29*, 992–1023.

[19] Tuckerman, M. E., Martyna, G. J., *J. Phys. Chem. B* 2000, *104*, 159–178.

[20] Glotzer, S. C., Paul, W., *Annu. Rev. Mater. Res.* 2002, *32*, 401–436.

[21] Lennard-Jones, J. E., *Proc. Phys. Soc.* 1931, *43*, 461–482.

[22] Arnold, A., Holm, C., *Adv. Polym. Sci.* 2005, *185*, 59–109.

[23] Deserno, M., Holm, C., *J. Chem. Phys.* 1998, *109*, 7678–7693.

[24] Greengard, L., Rokhlin, V., *J. Comput. Phys.* 1987, *73*, 325–348.

[25] Lee, F. S., Warshel, A., *J. Chem. Phys.* 1992, *97*, 3100–3107.

[26] Leach, A. R., *Molecular Modelling: Principles and Applications*, Addison Wesley Longman, Essex, England 1996.

[27] Binder, K., *Monte Carlo and Molecular Dynamics Simulations in Polymer Science*, Oxford University Press, New York, NY, USA 1995.

[28] Underhill, P. T., Doyle, P. S., *J. Non-Newtonian Fluid Mech.* 2003, *122*, 3–31.

[29] Weeks, J. D., Chandler, D., Andersen, H. C., *J. Chem. Phys.* 1978, *54*, 5237–5247.

[30] Grest, G. S., Kremer, K., *Phys. Rev. A* 1986, *33*, 3628–3631.

[31] Ryckaert, J.-P., Ciccotti, G., Berendsen, H. J. C., *J. Comput. Phys.* 1977, *23*, 327–341.

[32] Andersen, H. C., *J. Comput. Phys.* 1983, *52*, 24–34.

[33] Teraoka, I., *Polymer Solutions: An Introduction to Physical Properties*. Wiley, New York 2002.

[34] Berendsen, H. J. C., Postma, J. P. M., DiNola, A., Haak, J. R., *J. Chem. Phys.* 1984, *81*, 3684–3690.

[35] Andersen, H. C., *J. Chem. Phys.* 1980, *72*, 2384–2393.

[36] Stoyanov, S. D., Groot, R. D., *J. Chem. Phys.* 2005, *122*, 114112.

[37] Soddemann, T., Dünweg, B., Kremer, K., *Phys. Rev. E* 2003, *68*, 046702.

[38] Nosé, S., *J. Chem. Phys.* 1984, *81*, 511–519.

[39] Hoover, W. G., *Phys. Rev. A* 1985, *31*, 1695–1697.

[40] Lowe, C. P., *Europhys. Lett.* 1999, *47*, 145–151.

[41] Hunenberger, P. H., *Adv. Polym. Sci.* 2005, *173*, 105–147.

[42] Guillot, B., *J. Mol. Liq.* 2002, *101*, 219–260.

[43] Wallqvist, A., Mountain, R. D., *Rev. Comput. Chem.* 1999, *13*, 183–247.

[44] Head-Gordon, T., Hura, G., *Chem. Rev.* 2002, *102*, 2651–2670.

[45] Jorgensen, W. L., Tirado-Rives, J., *Proc. Natl. Acad. Sci. USA* 2005, *102*, 6665–6670.

[46] Dimitrov, D. I., Milchev, A., Binder, K., Heermann, D. W., *Macromol. Theory Simul.* 2006, *15*, 573–583.

[47] Hoogerbrugge, P. J., Koelman, J. M. V. A., *Europhys. Lett.* 1992, *19*, 155–160.

[48] Groot, R. D., Warren, P., *J. Chem. Phys.* 1997, *107*, 4423–4435.

[49] Español, P., *Phys. Rev. E* 1995, *52*, 1734–1742.

[50] Kong, Y., Manke, C. W., Madden, W. G., Schlijper, A. G., *J. Chem. Phys.* 1997, *107*, 592–602.

[51] Goujon, F., Malfreyt, P., Tildesley, D. J., *Mol. Phys.* 2005, *103*, 2675–2685.

[52] Malevanets, A., Kapral, R., *J. Chem. Phys.* 1999, *110*, 8605–8613.

[53] Malevanets, A., Kapral, R., *J. Chem. Phys.* 2000, *112*, 7260–7269.

[54] Yeomans, J. M., *Physica A* 2006, *369*, 159–184.

[55] Ripoll, M., Mussawisade, K., Winkler, R. G., Gompper, G., *Europhys. Lett.* 2004, *68*, 106–112.

[56] Ripoll, M., Mussawisade, K., Winkler, R. G., Gompper, G., *Phys. Rev. E* 2005, *72*, 016701.

[57] Inoue, Y., Chen, Y., Ohashi, H., *Comput. Phys. Commun.* 2001, *142*, 114–116.

[58] Inoue, Y., Chen, Y., Ohashi, H., *J. Comput. Phys.* 2004, *201*, 191–203.

[59] Pooley, C. M., Yeomans, J. M., *J. Phys. Chem. B* 2005, *109*, 6505–6513.

[60] Noguchi, H., Kikuchi, N., Gompper, G., *Europhys. Lett.* 2007, *78*, 10005.

[61] Ihle, T., Kroll, D. M., *Phys. Rev. E* 2001, *63*, 020201.

[62] Ihle, T., Kroll, D. M., *Phys. Rev. E* 2003, *67*, 066705.

[63] Malevanets, A., Yeomans, J. M., *Europhys. Lett.* 2000, *52*, 231–237.

[64] Kikuchi, N., Gent, A., Yeomans, J. M., *Eur. Phys. J. E Soft Matter* 2002, *9*, 63–66.

[65] Ripoll, M., Winkler, R. G., Gompper, G., *Phys. Rev. Lett.* 2006, *96*, 188302.

[66] Ali, I., Marenduzzo, D., Yeomans, J. M., *J. Chem. Phys.* 2004, *121*, 8635–8641.

[67] Mussawisade, K., Ripoll, M., Winkler, R. G., Gompper, G., *J. Chem. Phys.* 2005, *123*, 144905.

[68] Kikuchi, N., Ryder, J. F., Pooley, C. M., Yeomans, J. M., *Phys. Rev. E* 2005, *71*, 061804.

[69] Webster, M. A., Yeomans, J. M., *J. Chem. Phys.* 2005, *122*, 164903.

[70] Falck, E., Lahtinen, J. M., Vattulainen, I., Ala-Nissila, T., *Eur. Phys. J. E Soft Matter* 2004, *13*, 267–275.

[71] Padding, J. T., Louis, A. A., *Phys. Rev. Lett.* 2004, *93*, 220601.

[72] McNamara, G. R., Zanetti, G., *Phys. Rev. Lett.* 1988, *61*, 2332–2335.

[73] Raabe, D., *Modell. Simul. Mater. Sci. Eng.* 2004, *12*, R13–R46.

[74] Ahlrichs, P., Dünweg, B., *J. Chem. Phys.* 1999, *111*, 8225–8239.

[75] Usta, O. B., Ladd, A. J. C., Butler, J. E., *J. Chem. Phys.* 2005, *122*, 094902.

[76] Adhikari, R., Stratford, K., Cates, M. E., Wagner, A. J., *Europhys. Lett.* 2005, *71*, 473–479.

[77] Dünweg, B., Schiller, U. D., Ladd, A. J. C., *Phys. Rev. E* 2007, *76*, 036704.

[78] Coffey, W., Kalmykov, Y. P., Waldron, J. T., *The Langevin Equation*, World Scientific, River Edge, NJ 1996.

[79] Russel, W. B., Saville, D. A., Schowalter, W. R., *Colloidal Dispersions*, Cambridge University Press, Cambridge, UK 1992.

[80] Ermak, D., McCammon, J., *J. Chem. Phys.* 1978, *69*, 1352–1360.

[81] Doi, M., Edwards, S. F., *The Theory of Polymer Dynamics*, Clarendon Press, New York 1986.

[82] Ottinger, H. C., *Stochastic Processes in Polymeric Fluids: Tools and Examples for Developing Simulation Algorithms*, Springer, New York 1996.

[83] Graessley, W. W., *Polymeric Liquids & Networks: Dynamics and Rheology*, Taylor & Francis Group, New York 2008.

[84] Rotne, J., Prager, S., *J. Chem. Phys.* 1969, *50*, 4831–4837.

[85] Yamakawa, H., *Modern Theory of Polymer Solutions*, Harper & Row, New York 1971.

[86] Fixman, M., *Macromolecules* 1986, *19*, 1204–1207.

[87] Jendrejack, R. M., Graham, M. D., de Pablo, J. J., *J. Chem. Phys.* 2000, *113*, 2894–2900.

[88] Junghans, C., Praprotnik, M., Kremer, K., *Soft Matter* 2008, *4*, 156–161.

[89] Noguchi, H., Gompper, G., *Phys. Rev. E* 2008, *78*, 016706.

[90] Inoue, Y., Chen, Y., Ohashi, H., *J. Stat. Phys.* 2002, *107*, 85–100.

[91] Revenga, M., Zúñiga, I., Español, P., Pagonabarraga, I., *Int. J. Mod. Phys. C* 1998, *9*, 1319–1328.

[92] Smiatek, J., Allen, M. P., Schmid, F., *Eur. Phys. J. E Soft Matter* 2008, *26*, 115–122.

[93] Chen, S. Y., Martinez, D., Mei, R. W., *Phys. Fluids* 1996, *8*, 2527–2536.

[94] Ladd, A. J. C., Verberg, R., *J. Stat. Phys.* 2001, *104*, 1191–1251.

[95] Horbach, J., Succi, S., *Phys. Rev. Lett.* 2006, *96*, 224503.

[96] Chen, Y.-L., Ma, H., Graham, M. D., de Pablo, J. J., *Macromolecules* 2007, *40*, 5978–5984.

[97] Padding, J. T., Louis, A. A., *Phys. Rev. E* 2006, *74*, 031402.

[98] Madras, N., Sokal, A. D., *J. Stat. Phys.* 1988, *50*, 109–186.

[99] Leontidis, E., Forrest, B. M., Widmann, A. H., Suter, U. W., *J. Chem. Soc., Faraday Trans.* 1995, *91*, 2355–2368.

[100] de Pablo, J. J., Yan, Q. L., Escobedo, F. A., *Annu. Rev. Phys. Chem.* 1999, *50*, 377–411.

[101] Binder, K., Paul, W., *Macromolecules* 2008, *41*, 4537–4550.

[102] Newman, M. E. J., Barkema, G. T., *Monte Carlo Methods in Statistical Physics*, Oxford University Press, New York, USA 1999.

[103] Viovy, J.-L., *Rev. Mod. Phys.* 2000, *72*, 813–872.

[104] Landau, R. H., Paez, M. J., *Computational Physics : Problem Solving Using Computers*. Wiley Interscience, New York 1997.

[105] Gauthier, M. G., Slater, G. W., *J. Chem. Phys.* 2002, *117*, 6745–6756.

[106] Gauthier, M. G., Slater, G. W., *Phys. Rev. E* 2004, *70*, 015103.

[107] Gauthier, M. G., Slater, G. W., *Physica A* 2005, *355*, 283–296.

[108] Mercier, J. F., Slater, G. W., *J. Chem. Phys.* 1999, *110*, 6050–6056.

[109] Mercier, J. F., Slater, G. W., *J. Chem. Phys.* 1999, *110*, 6057–6065.

[110] Gauthier, M. G., Slater, G. W., Dorfman, K. D., *Eur. Phys. J. E Soft Matter* 2004, *15*, 71–82.

[111] Binder, K., Milchev, A., *J. Comput. Aided Mater. Des.* 2002, *9*, 33–74.

[112] Baumgärtner, A., Binder, K., *J. Chem. Phys.* 1979, *71*, 2541–2545.

[113] Verdier, P. H., Stockmayer, W. H., *J. Chem. Phys.* 1962, *36*, 227–235.

[114] Gurler, M. T., Crabb, C. C., Dahlin, D. M., Kovac, J., *Macromolecules* 1983, *16*, 398–403.

[115] Madras, N., Sokal, A., *J. Stat. Phys.* 1987, *47*, 573–595.

[116] Carmesin, I., Kremer, K., *Macromolecules* 1988, *21*, 2819–2823.

[117] Deutsch, H. P., Binder, K., *J. Chem. Phys.* 1991, *94*, 2294–2304.

[118] van Heukelum, A., Barkema, G. T., *Electrophoresis* 2002, *23*, 2562–2568.

[119] Deutsch, J. M., Reger, J. D., *J. Chem. Phys.* 1991, *95*, 2065–2071.

[120] Azuma, R., Takayama, H., *Phys. Rev. E* 1999, *59*, 650–655.

[121] Boileau, J., Slater, G. W., *Electrophoresis* 2001, *22*, 673–683.

[122] Gauthier, M. G., Slater, G. W., *J. Chem. Phys.* 2008, *128*, 065103.

[123] Keh, H. J., Tseng, H. C., *J. Colloid Interface Sci.* 2001, *242*, 450–459.

[124] Tessier, F., Slater, G. W., *Macromolecules* 2006, *39*, 1250–1260.

[125] Han, J., Craighead, H. G., *J. Vac. Sci. Technol. A* 1999, *17*, 2142–2147.

[126] Duong-Hong, D., Wang, J. -S., Liu, G. R., Chen, Y. Z., Han, J., Hadjiconstantinou, N. G., *Microfluid. Nanofluid.* 2007, *4*, 219–225.

[127] Guo, Z., Zhao, T. S., Shi, Y., *J. Chem. Phys.* 2005, *122*, 144907.

[128] Tessier, F., Slater, G. W., *Macromolecules* 2005, *38*, 6752–6754.

[129] Gaš, B., Kenndler, E., *Electrophoresis* 2000, *21*, 3888–3897.

[130] Štědrý, M., Gaš, B., Kenndler, E., *Electrophoresis* 1995, *16*, 2027–2033.

[131] Harden, J. L., Long, D., Ajdari, A., *Langmuir* 2001, *17*, 705–715.

[132] Qiao, R., He, P., *Langmuir* 2007, *23*, 5810–5816.

[133] Qiao, R., *Langmuir* 2006, *22*, 7096–7100.

[134] Muthukumar, M., *Electrophoresis* 1996, *17*, 1167–1172.

[135] Volkel, A. R., Noolandi, J., *J. Chem. Phys.* 1995, *102*, 5506–5511.

[136] Mohanty, U., Stellwagen, N. C., *Biopolymers* 1999, *49*, 209–214.

[137] Hoagland, D. A., Arvanitidou, E., Welch, C., *Macromolecules* 1999, *32*, 6180–6190.

[138] Cottet, H., Gareil, P., Theodoly, O., Williams, C. E., *Electrophoresis* 2000, *21*, 3529–3540.

[139] Stellwagen, E., Lu, Y. J., Stellwagen, N. C., *Biochemistry* 2003, *42*, 11745–11750.

[140] Yeh, I. C., Hummer, G., *Biophys. J.* 2004, *86*, 681–689.

[141] Yeh, I. C., Hummer, G., *J. Phys. Chem. B* 2004, *108*, 15873–15879.

[142] Frank, S., Winkler, R. G., *Europhys. Lett.* 2008, *83*, 38004.

[143] Grass, K., Boehme, U., Scheler, U., Cottet, H., Holm, C., *Phys. Rev. Lett.* 2008, *100*, 096104.

[144] Grass, K., Holm, C., *J. Phys.: Condens. Matter* 2008, *20*, 494217.

[145] Netz, R. R., *J. Phys. Chem. B* 2003, *107*, 8208–8217.

[146] Netz, R. R., *Phys. Rev. Lett.* 2003, *90*, 128104.

[147] Stellwagen, E., Stellwagen, N. C., *Electrophoresis* 2002, *23*, 2794–2803.

[148] Jendrejack, R. M., de Pablo, J. J., Graham, M. D., *J. Chem. Phys.* 2002, *116*, 7752–7759.

[149] Deutsch, J. M., *Science* 1988, *240*, 922–924.

[150] Deutsch, J. M., Madden, T. L., *J. Chem. Phys.* 1989, *90*, 2476–2485.

[151] Smith, S. B., Aldridge, P. K., Callis, J. B., *Science* 1989, *243*, 203–206.

[152] Schwartz, D. C., Koval, M., *Nature* 1989, *338*, 520–522.

[153] Nixon, G. I., Slater, G. W., *Phys. Rev. E* 1994, *50*, 5033–5038.

[154] Sevick, E. M., Williams, D. R. M., *Phys. Rev. Lett.* 1996, *76*, 2595–2598.

[155] Saville, P. M., Sevick, E. M., *Macromolecules* 1999, *32*, 892–899.

[156] André, P., Long, D., Ajdari, A., *Eur. Phys. J. B* 1998, *4*, 307–312.

[157] Randall, G. C., Doyle, P. S., *Macromolecules* 2006, *39*, 7734–7745.

[158] Kim, J. M., Doyle, P. S., *Macromolecules* 2007, *40*, 9151–9163.

[159] Holleran, S. P., Larson, R.G., *Macromolecules* 2008, *41*, 5042–5054.

[160] Holleran, S. P., Larson, R. G., *Rheol. Acta* 2008, *47*, 3–17.

[161] Kenward, M., Slater, G. W., *Eur. Phys. J. E Soft Matter* 2006, *20*, 125–141.

[162] Barron, A. E., Blanch, H. W., Soane, D. S., *Electrophoresis* 1994, *15*, 597–615.

[163] Hubert, S. J., Slater, G. W., Viovy, J.-L., *Macromolecules* 1996, *29*, 1006–1009.

[164] Starkweather, M. E., Muthukumar, M., Hoagland, D. A., *Macromolecules* 1998, *31*, 5495–5501.

[165] Starkweather, M. E., Muthukumar, M., Hoagland, D. A., *Macromolecules* 1999, *32*, 6837–6840.

[166] Slater, G. W., Guo, H. L., Electrophoresis 1996, 17, 977–988.

[167] Slater, G. W., Guo, H. L., Electrophoresis 1996, 17, 1407–1415.

[168] Labrie, J., Mercier, J.-F., Slater, G. W., Electrophoresis 2000, 21, 823–833.

[169] Mercier, J.-F., Tessier, F., Slater, G. W., Electrophoresis 2001, 22, 2631–2638.

[170] Dorfman, K. D., Slater, G. W., Gauthier, M. G., J. Chem. Phys. 2003, 119, 6979–6980.

[171] Gauthier, M. G., Slater, G. W., Electrophoresis 2003, 24, 441–451.

[172] Anselmetti, D., Duong, T. T., Eichhorn, R., Reimann, P., Regtmeier, J., Ros, A., Nature 2005, 436, 928.

[173] Tessier, F., Labrie, J., Slater, G. W., Macromolecules 2002, 35, 4791–4800.

[174] Tessier, F., Slater, G. W., Appl. Phys. A 2002, 75, 285–291.

[175] Han, J., Turner, S. W., Craighead, H. G., Phys. Rev. Lett. 1999, 83, 1688–1691.

[176] Griess, G. A., Rogers, E., Serwer, P., Electrophoresis 2001, 22, 981–989.

[177] Deamer, D. W., Akeson, M., Trends Biotechnol. 2000, 18, 147–151.

[178] Kasianowicz, J. J., Brandin, E., Branton, D., Deamer, D. W., Proc. Natl. Acad. Sci. USA 1996, 93, 13770–13773.

[179] Sung, W., Park, P. J., Phys. Rev. Lett. 1996, 77, 783–786.

[180] Muthukumar, M., J. Chem. Phys. 2003, 118, 5174–5184.

[181] Wolterink, J. K., Barkema, G. T., Panja, D., Phys. Rev. Lett. 2006, 96, 208301.

[182] Dubbeldam, J. L. A., Milchev, A., Rostiashvili, V. G., Vilgis, T. A., Phys. Rev. E 2007, 76, 010801.

[183] Storm, A. J., Storm, C., Chen, J., Zandbergen, H., Joanny, J.-F., Dekker, C., Nano Lett. 2005, 5, 1193–1197.

[184] Dekker, C., Nat. Nanotechnol. 2007, 2, 209–215.

[185] Zwolak, M., Ventra, M. D., Rev. Mod. Phys. 2008, 80, 141–165.

[186] Soni, G. V., Meller, A., Clin. Chem. 2007, 53, 1996–2001.

[187] Li, J., Gershow, M., Stein, D., Brandin, E., Golovchenko, J. A., Nat. Mater. 2003, 2, 611–615.

[188] Meller, A., Nivon, L., Branton, D., Phys. Rev. Lett. 2001, 86, 3435–3438.

[189] Muthukumar, M., J. Chem. Phys. 1999, 111, 10371–10374.

[190] Chuang, J., Kantor, Y., Kardar, M., Phys. Rev. E 2002, 65, 011802.

[191] Kantor, Y., Kardar, M., Phys. Rev. E 2004, 69, 021806.

[192] Panja, D., Barkema, G. T., Biophys. J. 2008, 94, 1630–1637.

[193] Luo, K., Ala-Nissila, T., Ying, S. C., J. Chem. Phys. 2006, 124, 034714.

[194] Chern, S. S., Cardenas, A. E., Coalson, R. D., J. Chem. Phys. 2001, 115, 7772–7782.

[195] Chen, C. M., Physica A 2005, 350, 95–107.

[196] Milchev, A., Binder, K., Bhattacharya, A., J. Chem. Phys. 2004, 121, 6042–6051.

[197] Gauthier, M. G., Slater, G. W., J. Chem. Phys. 2008, 128, 205103.

[198] Mathé, J., Aksimentiev, A., Nelson, D. R., Schulten, K., Meller, A., Proc. Natl. Acad. Sci. USA 2005, 102, 12377–12382.

[199] Guo, L., Luijten, E., Springer Proc. Phys. 2007, 105, 159–164.

[200] Tian, P., Smith, G. D., J. Chem. Phys. 2003, 119, 11475–11483.

[201] Huopaniemi, I., Luo, K., Ala-Nissila, T., Ying, S. C., J. Chem. Phys. 2006, 125, 124901.

[202] Guillouzic, S., Slater, G. W., Phys. Lett. A 2006, 359, 261–264.

[203] Gauthier, M. G., Slater, G. W., Eur. Phys. J. E. Soft matter 2008, 25, 17–23.

[204] Lansac, Y., Maiti, P. K., Glaser, M. A., Polymer 2004, 45, 3099–3110.

[205] Izmitli, A., Schwartz, D. C., Graham, M. D., de Pablo, J. J., J. Chem. Phys. 2008, 128, 085102.

[206] Fyta, M., Kaxiras, E., Melchionna, S., Succi, S., Comput. Sci. Eng. 2008, 10, 10–19.

[207] He, Y. D., Qian, H. J., Lu, Z. Y., Li, Z. S., Polymer 2007, 48, 3601–3606.

[208] Ali, I., Yeomans, J. M., J. Chem. Phys. 2005, 123, 234903.

[209] Wei, D., Yang, W., Jin, X., Liao, Q., J. Chem. Phys. 2007, 126, 204901.

[210] Luo, K., Ala-Nissila, T., Ying, S. C., Bhattacharya, A., Phys. Rev. Lett. 2007, 99, 148102.

[211] Kong, C. Y., Muthukumar, M., Electrophoresis 2002, 23, 2697–2703.

[212] Ambjornsson, T., Apell, S. P., Konkoli, Z., Marzio, E. A. D., Kasianowicz, J. J., J. Chem. Phys. 2002, 117, 4063–4073.

[213] Luo, K., Ala-Nissila, T., Ying, S. C., Bhattacharya, A., J. Chem. Phys. 2007, 126, 145101.

[214] Gauthier, M., Slater, G. W., J. Chem. Phys. 2008, 128, 175103.

[215] Huopaniemi, I., Luo, K., Ala-Nissila, T., Ying, S. C., Phys. Rev. E 2007, 75, 061912.

[216] Luo, K., Huopaniemi, I., Ala-Nissila, T., Ying, S. C., J. Chem. Phys. 2006, 124, 114704.

[217] Dubbeldam, J. L. A., Milchev, A., Rostiashvili, V. G., Vilgis, T. A., Europhys. Lett. 2007, 79, 18002.

[218] Baumgärtner, A., Muthukumar, M., J. Chem. Phys. 1987, 87, 3082–3088.

[219] Muthukumar, M., Baumgärtner, A., Macromolecules 1989, 22, 1941–1946.

[220] Baumgärtner, A., Muthukumar, M., Adv. Chem. Phys. 1996, XCIV, 625–708.

[221] Rousseau, J., Drouin, G., Slater, G. W., Phys. Rev. Lett. 1997, 79, 1945–1948.

[222] Han, J., Craighead, H. G., Science 2000, 288, 1026–1029.

[223] Han, J., Craighead, H. G., *Anal. Chem.* 2002, *74*, 394–401.

[224] Chen, Z., Escobedo, F. A., *Mol. Simul.* 2003, *29*, 417–425.

[225] de Pablo, J. J., Laso, M., Suter, U. W., *J. Chem. Phys.* 1992, *96*, 2395–2403.

[226] Streek, M., Schmid, F., Duong, T. T., Ros, A., *J. Biotechnol.* 2004, *112*, 79–89.

[227] Streek, M., Schmid, F., Duong, T. T., Anselmetti, D., Ros, A., *Phys. Rev. E* 2005, *71*, 011905.

[228] Panwar, A. S., Kumar, S., *Macromolecules* 2006, *39*, 1279–1289.

[229] Lee, Y. M., Joo, Y. L., *J. Chem. Phys.* 2007, *127*, 124902.

[230] Pernodet, N., Samuilov, V., Shin, K., Sokolov, J., Rafailovich, M. H., Gersappe, D., Chu, B., *Phys. Rev. Lett.* 2000, *85*, 5651–5654.

[231] Seo, Y. S., Samuilov, V. A., Sokolov, J., Rafailovich, M., Tinland, B., Kim, J., Chu, B., *Electrophoresis* 2002, *23*, 2618–2625.

[232] Luo, H. B., Gersappe, D., *Electrophoresis* 2002, *23*, 2690–2696.

[233] Seo, Y. S., Luo, H., Samuilov, V. A., Rafailovich, M. H., Sokolov, J., Gersappe, D., Chu, B., *Nano Lett.* 2004, *4*, 659–664.

[234] Li, B. Q., Fang, X. H., Luo, H. B., Petersen, E., Seo, Y. S., Samuilov, V., Rafailovich, M. *et al.*, *Electrophoresis* 2006, *27*, 1312–1321.

[235] Reichhardt, C. J. O., Reichhardt, C., *Phys. Rev. E* 2006, *74*, 051908.

[236] Hoda, N., Kumar, S., *Langmuir* 2007, *23*, 11747–11760.

[237] Odom, T. W., Thalladi, V. R., Love, J. C., Whitesides, G. M., *J. Am. Chem. Soc.* 2002, *124*, 12112–12113.

[238] Kan, C. W., Fredlake, C. P., Doherty, E. A. S., Barron, A. E., *Electrophoresis* 2004, *25*, 3564–3588.

[239] Fredrickson, C. K., Fan, Z. H., *Lab Chip* 2004, *4*, 526–533.

[240] Reisner, W., Morton, K. J., Riehn, R., Wang, Y. M., Yu, Z. N., Rosen, M., Sturm, J. C. *et al.*, *Phys. Rev. Lett.* 2005, *94*, 196101.

[241] Krishnan, M., Moench, I., Schwille, P., *Nano Lett.* 2007, *7*, 1270–1275.

[242] Pennathur, S., Santiago, J. G., *Anal. Chem.* 2005, *77*, 6782–6789.

[243] Pennathur, S., Baldessari, F., Santiago, J. G., Kattah, M. G., Steinman, J. B., Utz, P. J., *Anal. Chem.* 2007, *79*, 8316–8322.

[244] Balducci, A., Mao, P., Han, J., Doyle, P. S., *Macromolecules* 2006, *39*, 6273–6281.

[245] Zheng, J. J., Yeung, E. S., *Anal. Chem.* 2002, *74*, 4536–4547.

[246] Zheng, J. J., Yeung, E. S., *Anal. Chem.* 2003, *75*, 3675–3680.

[247] Chen, Y. L., Graham, M. D., de Pablo, J. J., Randall, G. C., Gupta, M., Doyle, P. S., *Phys. Rev. E* 2004, *70*, 060901.

[248] Chen, Y. L., Graham, M. D., de Pablo, J. J., Jo, K., Schwartz, D. C., *Macromolecules* 2005, *38*, 6680–6687.

[249] Jendrejack, R. M., Dimalanta, E. T., Schwartz, D. C., Graham, M. D., de Pablo, J. J., *Phys. Rev. Lett.* 2003, *91*, 038102.

[250] Jendrejack, R. M., Schwartz, D. C., Graham, M. D., de Pablo, J. J., *J. Chem. Phys.* 2003, *119*, 1165–1173.

[251] Jendrejack, R. M., Schwartz, D. C., de Pablo, J. J., Graham, M. D., *J. Chem. Phys.* 2004, *120*, 2513–2529.

[252] Hernandez-Ortiz, J. P., Ma, H., de Pablo, J. J., Graham, M. D., *Phys. Fluids* 2006, *18*, 123101.

[253] Usta, O. B., Butler, J. E., Ladd, A. J. C., *Phys. Fluids* 2006, *18*, 031703.

[254] Usta, O. B., Butler, J. E., Ladd, A. J. C., *Phys. Rev. Lett.* 2007, *98*, 098301.

[255] Mathé, J., Di Meglio, J.-M., Tinland, B., *J. Colloid Interface Sci.* 2007, *316*, 831–835.

[256] Mathé, J., Di Meglio, J.-M., Tinland, B., *J. Colloid Interface Sci.* 2008, *322*, 315–320.

[257] Cross, J. D., Strychalski, E. A., Craighead, H. G., *J. Appl. Phys.* 2007, *102*, 024514.

[258] Pennathur, S., Santiago, J. G., *Anal. Chem.* 2005, *77*, 6772–6781.

[259] Delgado-Buscalioni, R., De Fabritiis, G., *Phys. Rev. E* 2007, *76*, 036709.

[260] Barsky, S., Delgado-Buscalioni, R., Coveney, P. V., *J. Chem. Phys.* 2004, *121*, 2403–2411.

[261] Dupuis, A., Kotsalis, E. M., Koumoutsakos, P., *Phys. Rev. E* 2007, *75*, 046704.

[262] Williams, S. A., Bell, J. B., Garcia, A. L., *Multiscale Model. Simul.* 2008, *6*, 1256–1280.

[263] Praprotnik, M., Delle Site, L., Kremer, K., *Annu. Rev. Phys. Chem.* 2008, *59*, 545–571.

[264] Delgado-Buscalioni, R., Kremer, K., Praprotnik, M., *J. Chem. Phys.* 2008, *128*, 114110.

[265] Müller-Plathe, F., *Soft Materials* 2002, *1*, 1–31.

[266] Chiesl, T. N., Forster, R. E., Root, B. E., Larkin, M., Barron, A. E., *Anal. Chem.* 2007, *79*, 7740–7747.

[267] Fredlake, C. P., Hert, D. G., Kan, C. W., Chiesl, T. N., Root, B. E., Forster, R. E., Barron, A. E., *Proc. Natl. Acad. Sci. USA* 2008, *105*, 476–481.

[268] Heller, C., Slater, G. W., Mayer, P., Dovichi, N., Pinto, D., Viovy, J. L., Drouin, G., *J. Chromatogr. A* 1998, *806*, 113–121.

[269] Ren, H., Karger, A. E., Oaks, F., Menchen, S., Slater, G. W., Drouin, G., *Electrophoresis* 1999, *20*, 2501–2509.

[270] Desruisseaux, C., Long, D., Drouin, G., Slater, G. W., *Macromolecules* 2001, *34*, 44–52.

[271] Haynes, R. D., Meagher, R. J., Won, J. I., Bogdan, F. M., Barron, A. E., *Bioconjugate Chem.* 2005, *16*, 929–938.

[272] Grosser, S. T., Savard, J. M., Schneider, J. W., *Anal. Chem.* 2007, *79*, 9513–9519.

[273] Savard, J. M., Grosser, S. T., Schneider, J. W., *Electrophoresis* 2008, *29*, 2779–2789.

[274] Knotts IV, T. A., Rathore, N., Schwartz, D. C., de Pablo, J. J., *J. Chem. Phys.* 2007, *126*, 084901.

[275] Van Der Spoel, D., Lindahl, E., Hess, B., Groenhof, G., Mark, A. E., Berendsen, H. J., *J. Comput. Chem.* 2005, *26*, 1701–1718.

[276] Brooks, B. R., Bruccoleri, R. E., Olafson, B. D., States, D. J., Swaminathan, S., Karplus, M., *J. Comput. Chem.* 1983, *4*, 187–217.

[277] Phillips, J. C., Braun, R., Wang, W., Gumbart, J., Tajkhorshid, E., Villa, E., Chipot, C. *et al.*, *J. Comput. Chem.* 2005, *26*, 1781–1802.

[278] Case, D. A., Cheatham, T. E., Darden, T., Gohlke, H., Luo, R., Merz, K. M., Onufriev, A. *et al.*, *J. Comput. Chem.* 2005, *26*, 1668–1688.

[279] Smith, W., Young, C., Rodger, P., *Mol. Simul.* 2002, *28*, 385–471.

[280] Plimpton, S. J., *J. Comput. Phys.* 1995, *117*, 1–19.

[281] Limbach, H. J., Arnold, A., Mann, B. A., Holm, C., *Comput. Phys. Commun.* 2006, *174*, 704–727.

6 Appendix

MD simulation packages

While the theory behind an MD simulation is conceptually straightforward, in practice it can be a large undertaking to code from scratch. This is particularly true when one wishes to implement more involved algorithms in order to efficiently calculate long-ranged electrostatic interactions or incorporate mesoscopic fluid models. For this reason, there exists a multitude of simulation "packages" in which the routines necessary for performing the simulation have already been implemented. Hence, the user can simply supply input information pertaining to their system, select simulation features and parameters, and then use the packages to execute the simulation, produce trajectory files, and, frequently, perform analysis. Thus, to aid the interested reader, we present in this appendix a table of the more prominent MD simulation packages (note that the list given here is by no means exhaustive; see, for example, the Wikipedia article on MD at http://en.wikipedia.org/w/index.php?title=Molecular_Dynamics&oldid=231786544).

In addition to providing the simulation package name (and related references), we also include some details for each package. The information given here is meant to convey what the package is most often used for and also to indicate any special features unique to this package. These entries should not be interpreted as restrictive, but rather as highlighting interesting or distinct features among a group of software which all accomplish similar goals.

For example, consider delineating the packages between "atomistic" or "coarse-grained" simulations. In principle, all the cited packages are capable of performing fully atomistic simulations. But as such simulations require a fully atomistic force field it is easiest to start with a package that either comes with some force fields implemented (the first four packages in the list) or, at least, is designed to be compatible with the force fields from other packages (the next two entries). Similarly, all of the packages could be used for coarse-grained simulations. In fact, due to its efficiency in calculating non-bonded interactions, GROMACS, a biomolecule-oriented package, has been used for coarse-grained polymer simulation work. However, in choosing a more coarse-grained oriented package, one is more likely to find other useful elements such as the implementation of mesoscopic fluid models as found in the last two entries.

Finally, we include a "Free" column. A check mark here indicates that the program is free for academic use (at a minimum). This column is included to encourage the interested reader to download and begin experimenting without any monetary investment.

Name[a]	Details	Free
GROMACS [275] www.gromacs.org	Includes force fields for fully atomistic. Efficient calculation of non-bonded interaction	✔
CHARMM [276] www.charmm.org	Includes force fields for fully atomistic. Pioneer for MD simulations	
NAMD [277] www.ks.uiuc.edu/Research/namd/	Includes force fields for fully atomistic. Capable of steered and interactive MD	✔
AMBER [278] amber.scripps.edu	Includes force fields for fully atomistic. AMBER force field is compatible with and used in many of these MD packages	
DL_Poly [279] www.ccp5.ac.uk/DL_POLY/	Compatible with GROMACS or AMBER force fields. Includes potentials for non-biological materials	✔
LAMMPS [280] lammps.sandia.gov	Compatible with CHARMM, AMBER, and GROMACS force fields. Includes DPD	✔
ESPResSo [281] www.espresso.mpg.de	Designed for coarse-grained. Includes many algorithms for electrostatics. Includes LB, DPD	✔

a) Parallelized versions of all these packages exist to take advantage of high performance computing clusters.